Presentation by Cesar La Hoz

IFT All-hands meeting

30 November 2012

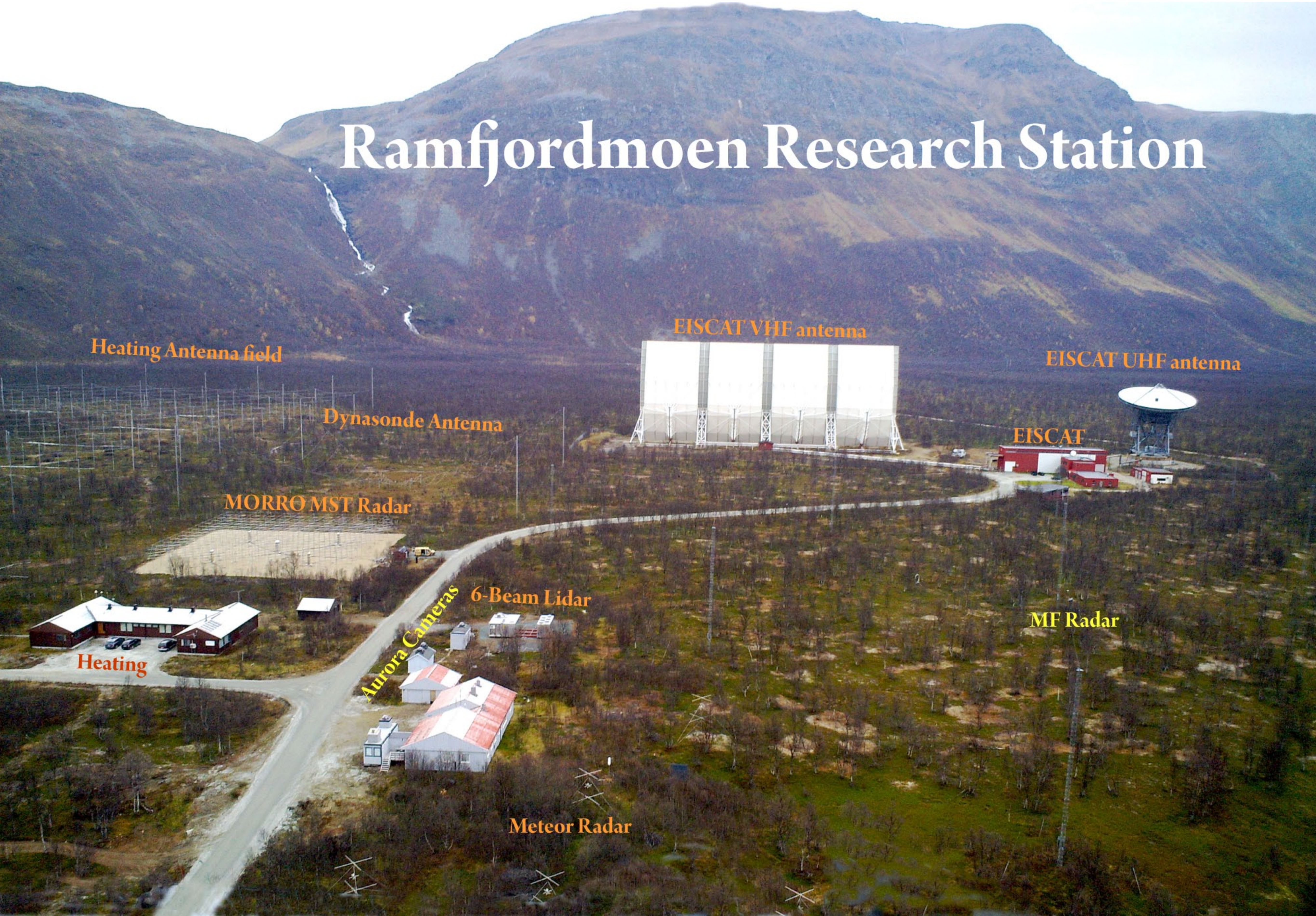
Ramfjordmoen Research Station
EISCAT VHF antenna
Heating Antenna field
EISCAT UHF antenna
Dynasonde Antenna
EISCAT
MORRO MST Radar
6-Beam Lidar
Aurora Cameras
MF Radar
Heating
Meteor Radar


MORRO
26th October 2007

EISCAT facilities

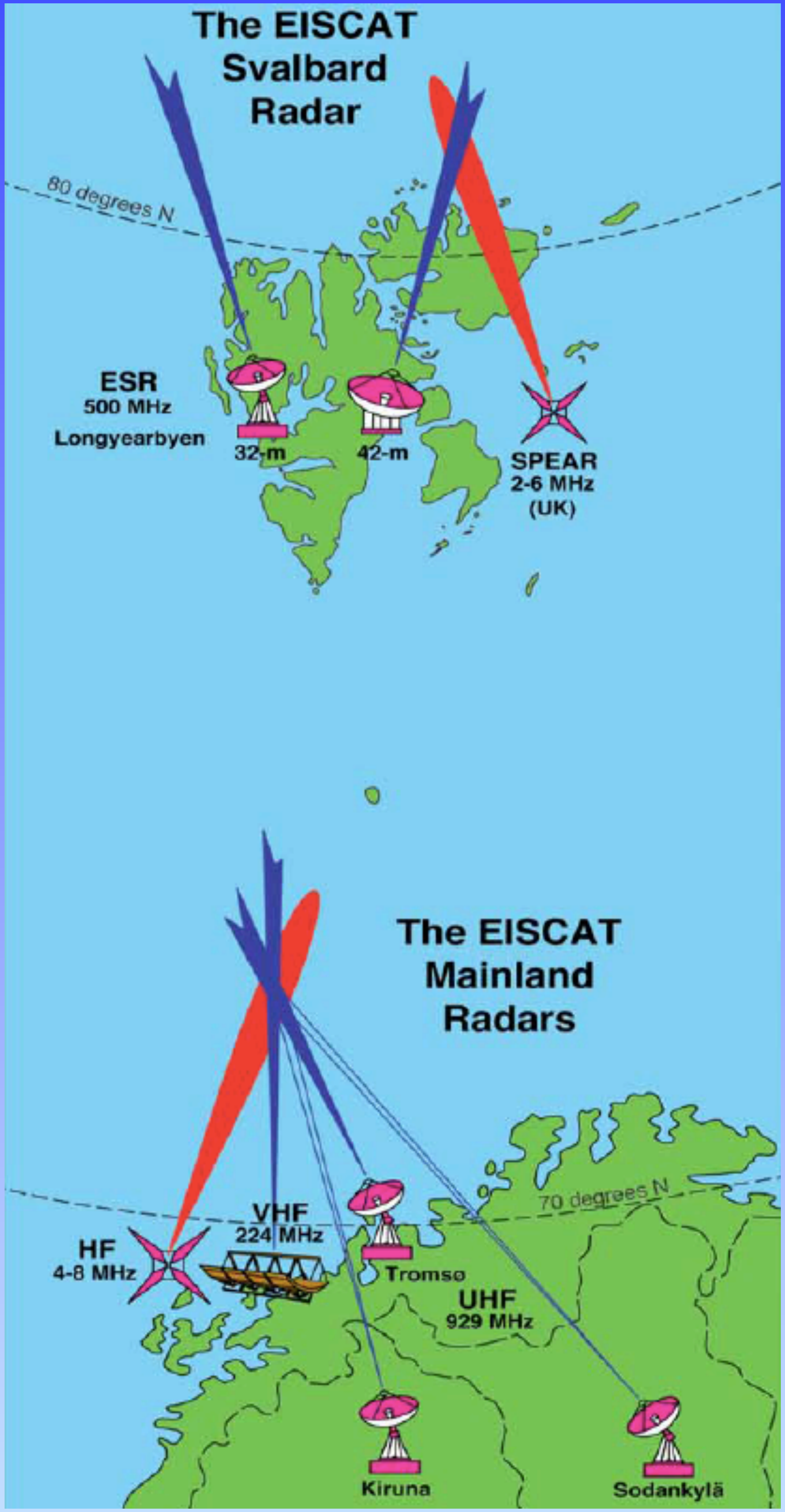

EISCAT Scientific Association operates currently three incoherent scatter radars in Northern Scandinavia on behalf of its associate members in Finland, China, Germany, Japan, Norway, Sweden and United Kingdom, as well as currently supporting partners in France, Russia and Ukraine. The current facilities include the 2-dish monostatic radar at 500Mhz at Longyearbyen, Svalbard, the 224 MHz monostatic VHF radar inTromsø, Norway, a tristatic UHF radar at 930 Mhz with transmitter/receiver in Tromsø and receivers in Kiruna, Sweden and Sodankylä, Finland, a high-power HF heating facility in Tromso, as well as 2 dynasondes in Tromso and at Svalbard.

EISCAT Group (part of the Space Physics Group)

- Prof. Unni Pia Løvhaug
- Prof. Cesar La Hoz
- Researcher Vasyl Belyey
- Postdoc Hannah Vickers
- PhD student Henry Pinedo
- PhD student Lindis Bjoland
- (PhD student Tim Dunker)
- Prof. emeritus Ove Havnes
- Prof. emeritus Asgeir Brekke

Research Projects

- PMSE/PMWE with EISCAT and MORRO (Ove+Henry).
- Imaging with the ESR: ESR Aperture Synthesis Imaging (EASI) project (Vasyl + Unni ++)
- Aperture Synthesis Imaging Radar (ASIR) for EISCAT_3D (Vasyl)
- One solar cycle of the ionosphere over Svalbard (Lindis+Unni)
- Neutral density measurements with Svalbard (Hannah+MK)
- Electron heating in the mesosphere (Henry)

Neutral Density Measurements in Svalbard (Hannah + MK)

ESR

Neutral density measurements in Svalbard (Hannah+MK) – 1

General ion momentum equation – field-aligned motion

$$\frac{\partial \vec{V}_{i\|}}{\partial t}+\left(\vec{V}_{i\|}\cdot\frac{\partial}{\partial s}\right)\vec{V}_{i\|}=-\frac{1}{n_i m_i}\frac{\partial P_{i\|}}{\partial s}+\frac{k_B}{m_i}\left(T_{i\|}-T_{i\perp}\right)\frac{1}{|\vec{B}|}\frac{\partial|\vec{B}|}{\partial s}+\frac{1}{n_i m_i}\frac{\partial \vec{\tau}_{i\|}}{\partial s}-\vec{g}_{\|}+\frac{e}{m_i}\vec{E}_{\|}$$
$$-\frac{(Q_i-L_i)}{n_i}\left(\vec{V}_{i\|}-V_{n\|}\right)-\nu_{in}\left(\vec{V}_{i\|}-\vec{V}_{n\|}\right)-\nu_{ie}\left(\vec{V}_{i\|}-\vec{V}_{e\|}\right)+\frac{z_{in}\nu_{in}}{n_i k_B T_{in\|}}\left(\vec{q}_{i\|}-\frac{n_i m_i}{n_n m_n}\vec{q}_{n\|}\right)+\frac{3}{5}\frac{m_e\nu_{ie}}{n_i m_i k_B T_{e\|}}\left(\vec{q}_{i\|}-\frac{n_i m_i}{n_e m_e}\vec{q}_{e\|}\right)$$

Neglect:
- Advection (small for subsonic ion flow)
- Magnetic mirror force (small in the topside ionosphere)
- Height differential of the stress tensor (small in the vertical direction)
- Chemical reactions (small in the topside)
- **Joule heating**
- **Heat flux of ions and electrons**

$\}$ **for quiet conditions consider only Kp < 2 data**

Keep:
- Ion pressure gradient (upward in the topside) $P_{i\|}=n_i k_B T_{i\|}$
- Electron pressure gradient (upward) $\vec{E}_{\|}=-\frac{1}{n_e e}\frac{\partial P_{e\|}}{\partial s}-\frac{m_i\nu_{ie}}{e}\left(\vec{V}_{e\|}-\vec{V}_{i\|}\right)+\frac{3}{5}\frac{m_i\nu_{ie}}{n_e e k_B T_{e\|}}\vec{q}_{e\|}$
- Gravity (downward) $\vec{g}_{\|}=g_s\sin(I)$

Simplified ion momentum equation

$$\nu_{in}=-\frac{1}{V_{i\|}}\left(g\sin I+\frac{k_B}{n_e m_i}\frac{\partial}{\partial s}\{n_e(T_{e\|}+T_{i\|}\}\right)$$

Estimate with incoherent scatter plasma parameters

$$\nu_{in}=3.67\times10^{-17}n_n\sqrt{T_{in}}\left(1-0.064\log_{10}T_{in}\right)^2$$

(Schunk and Nagy, 2000)

$$\rightarrow n_n=\frac{\nu_{in}}{3.67x10^{-17}\sqrt{T_{in}}(1-0.064log_{10}T_{in})^2}$$

For O only

Assumptions

- Steady state (dVi/dt = 0) and no Joule heating ie. $T_i = T_n = T_{in}$
- Vertical neutral winds at high latitudes are small i.e. < 15m s^{-1} during low activity (Aruliah and Rees, 1995). Uusally average to 0 over night-time → we assume $V_n = 0$

Neutral density measurements in Svalbard (Hannah+MK) – 2

Submitted for Publication

Results

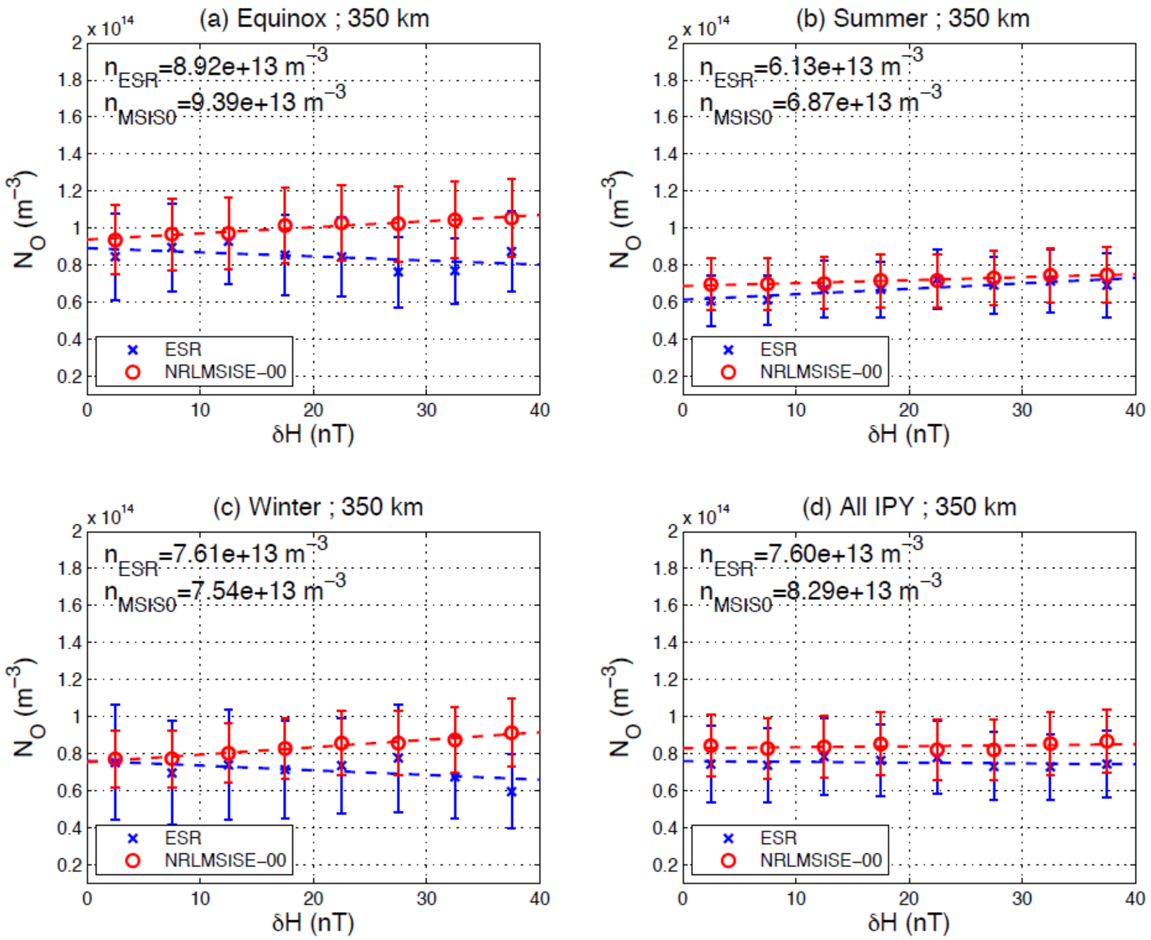

|ΔH|-binned ESR and MSIS estimates of atomic oxygen density for 350 km

- (a) Equinox: Mar, Apr, Sep, Oct;
- (b) Summer: May, Jun, Jul, Aug;
- (c) Winter: Nov, Dec, Jan, Feb;
- (d) Entire IPY dataset

Height of best agreement between the 'zero activity' estimates (ESR_0 and $MSIS_0$) derived from extrapolation of linear fit at 350 km.

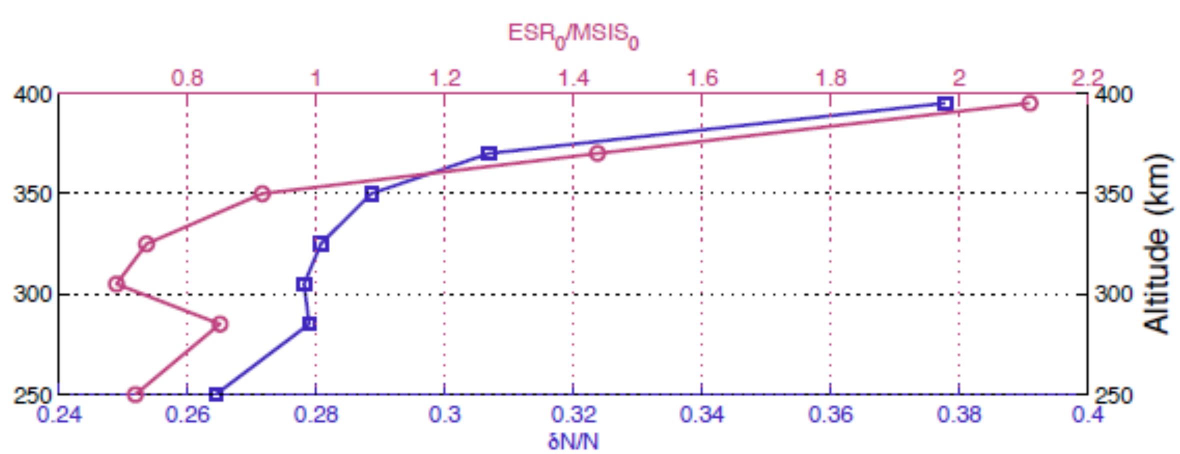

- Altitude profile for (pink) ESR_0 / $MSIS_0$ i.e. the ratio of zero activity densities and (blue) the median fractional error in density for lowest activity level
- Smallest error at 250 km due to highest SNR but only ~2% increase in error at altitude where ESR_0 / $MSIS_0$ ≈ 1

Electron Heating in the Mesosphere (Henry)

EISCAT
MORRO

Electron heating in the mesosphere (Henry) – 1

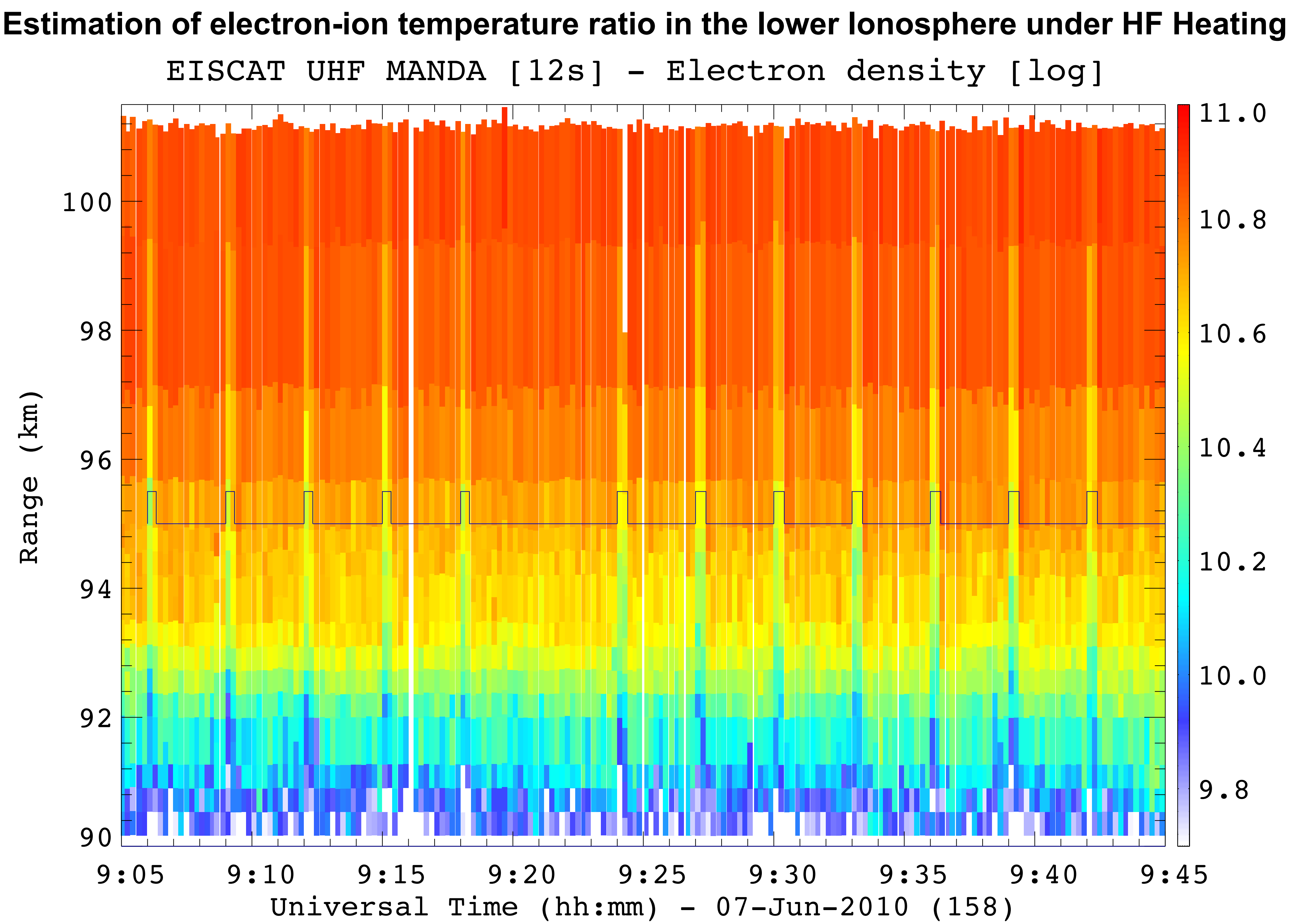

$$P_{radar} = \frac{C_{SYS}}{R^2}\left(\frac{\sigma_e}{(1+\alpha^2)(1+(T_e/T_i)+\alpha^2)}\right)N_e \qquad (T_e/T_i)_{ON} = 2\frac{(N_e)_{OFF}}{(N_e)_{ON}} - 1$$

Electron heating in the mesosphere (Henry) – 2

Estimation of electron-ion temperature ratio in the lower Ionosphere under HF Heating

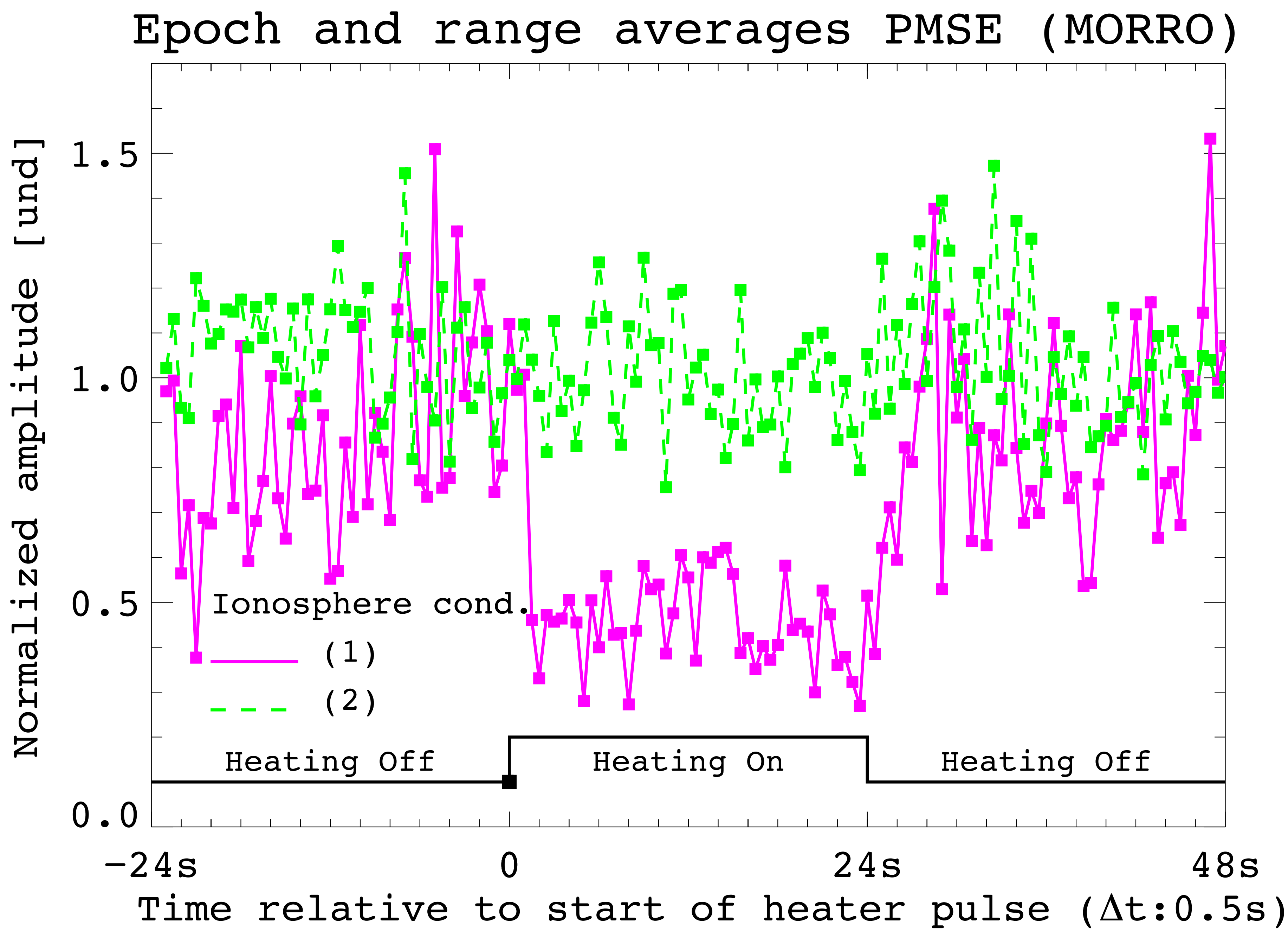

(1) Quiet ionosphere:

Between 09:05-09:45UT and 85-86km

(2) Particle precipitation (larger electron density in D-region)

Between 11:05-11:45UT and 84-85km

One solar cycle of the ionosphere above Svalbard
(Lindis, Vasyl, Unni)

ESR

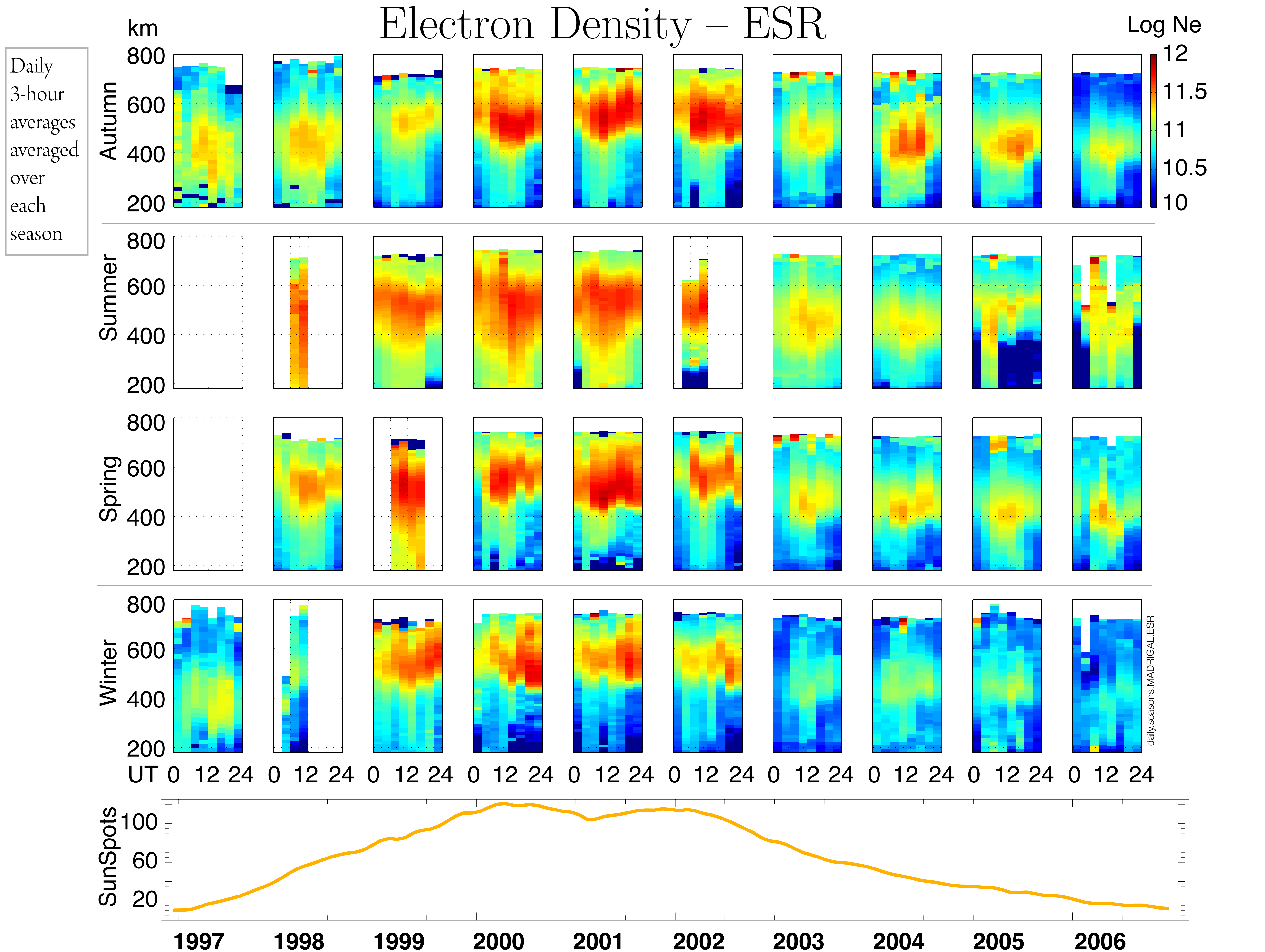

Electron Density – ESR
km
Log Ne
12
11.5
11
10.5
10
Daily
3-hour
averages
averaged
over
each
season
Autumn
Summer
Spring
Winter
800
600
400
200
UT 0 12 24
daily.seasons.MADRIGAL.ESR
SunSpots
100
60
20
1997
1998
1999
2000
2001
2002
2003
2004
2005
2006

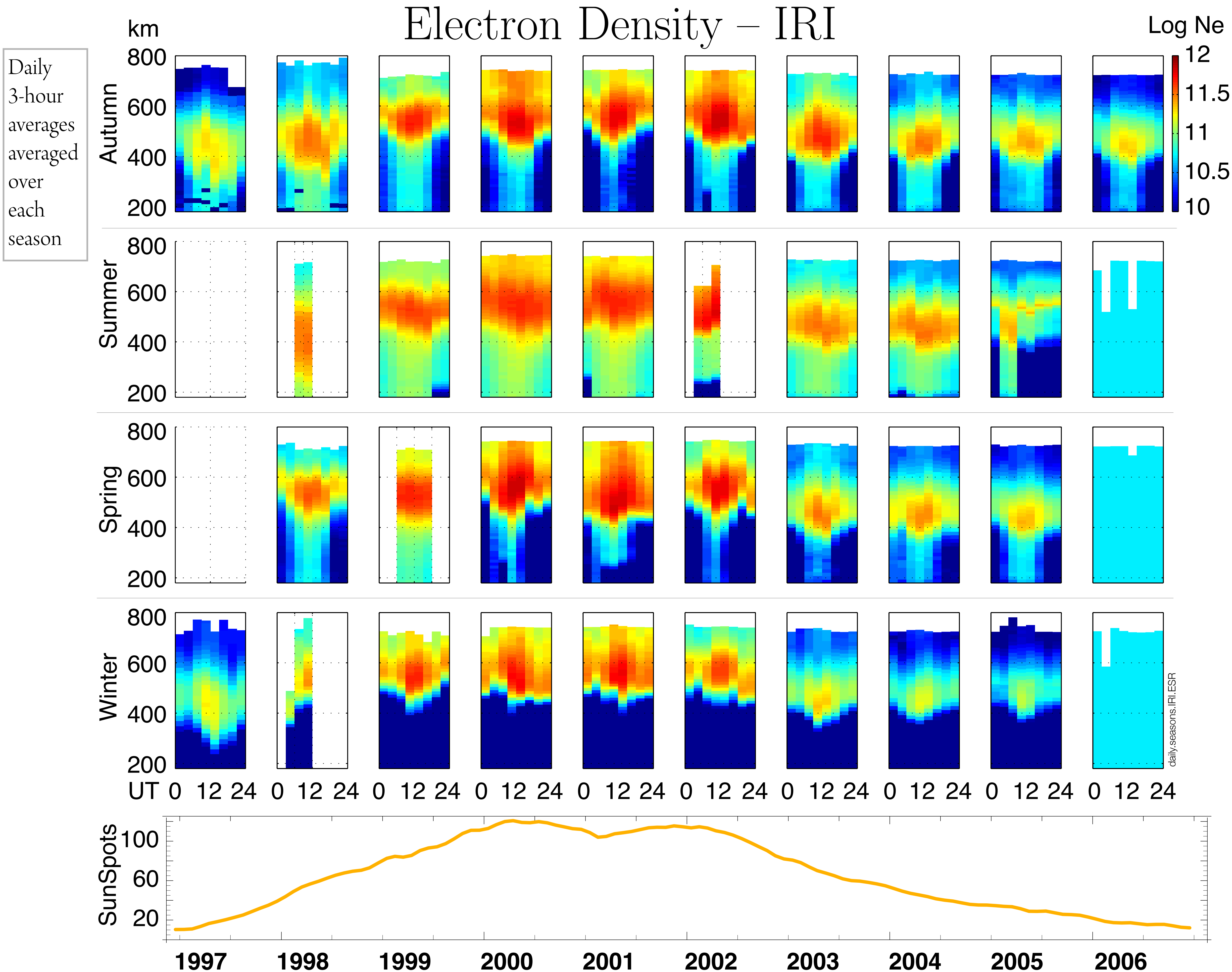

Electron Density – IRI
km
Log Ne
Daily
3-hour
averages
averaged
over
each
season
Autumn
Summer
Spring
Winter
800
600
400
200
12
11.5
11
10.5
10
UT 0 12 24
SunSpots
100
60
20
1997
1998
1999
2000
2001
2002
2003
2004
2005
2006
daily.seasons.IRI.ESR

Electron Density – ESR/IRI

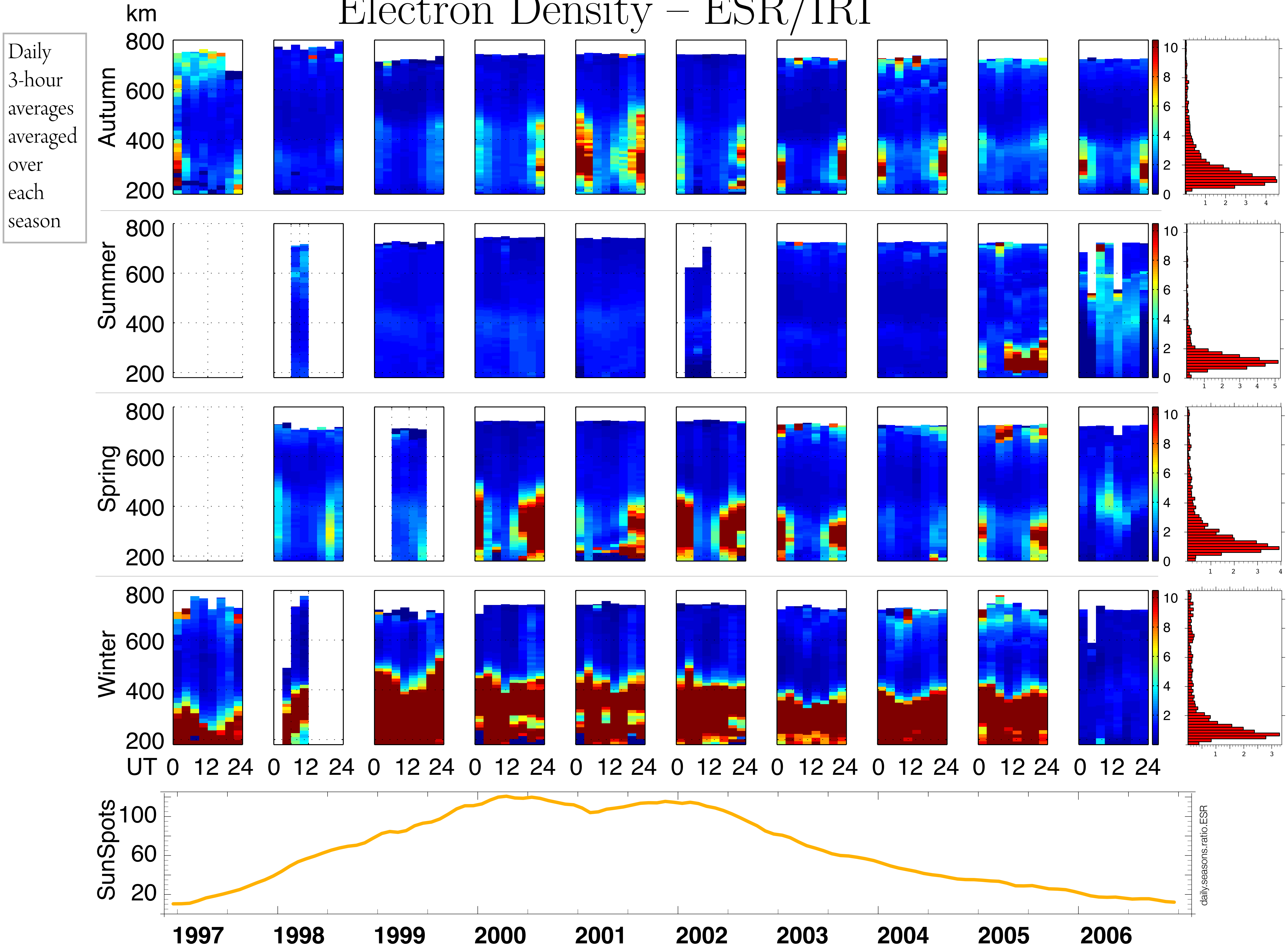

```
Histogram[Drop[Drop[Sort[ratioEsrIri], ]1500], 170]];
```

distributionAll

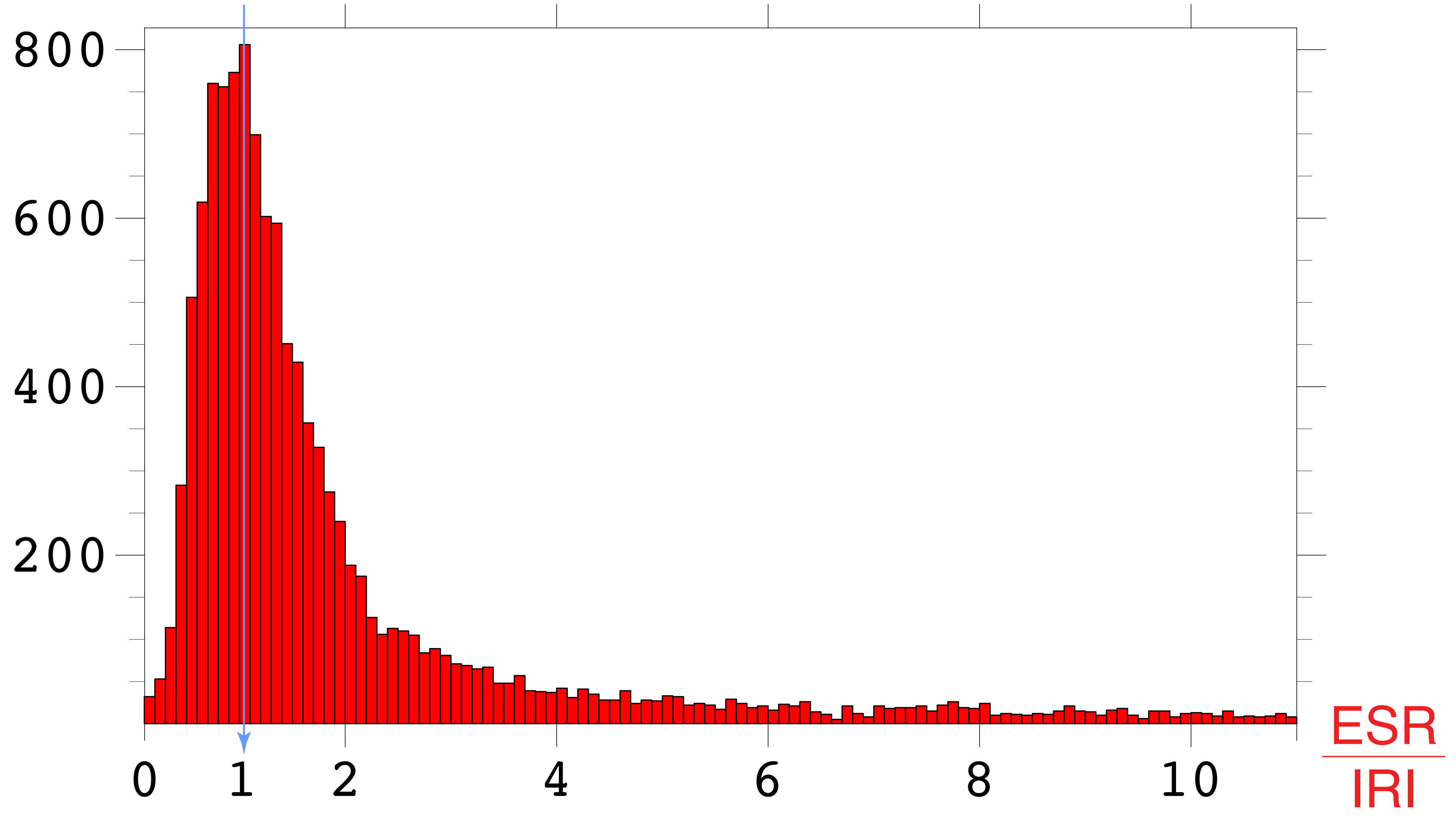


```
DispersionReport[Drop[Drop[Sort[ratioEsrIri], ]1500], 170]]
```

{Variance = 3.80128, StandardDeviation = 1.94969,
SampleRange = 10.8717, MeanDeviation = 1.2897,
MedianDeviation = 0.491853, QuartileDeviation = 0.582976}

Polar Mesospheric Summer Echoes
(Henry + Ove)

PMSE
KIRUNA

Multi-frequency PMSE observations Summer 2011

1	930 MHz	16 cm	UHF	EISCAT	Tromsø	IS
2	254 MHz	67 cm	VHF	EISCAT	Tromsø	IS
3	254 MHz	82 cm	VHF	EISCAT	Kiruna	Bi-static IS
4	54 MHz	278 cm	VHF	MORRO	Tromsø	MST
5	8 MHz	19 m	HF	Heater	Tromsø	Diagnostic HF
6	5.423 MHz		RF	Heater	Tromsø	Modifier HF

Multi-frequency PMSE observations Summer 2011

1	930 MHz	16 cm	UHF	EISCAT Tromsø	IS
2	254 MHz	67 cm	VHF	EISCAT Tromsø	IS
3	254 MHz	82 cm	VHF	EISCAT Kiruna	Bi-static IS
4	54 MHz	278 cm	VHF	MORRO Tromsø	MST
5	8 MHz	19 m	HF	Heater Tromsø	Diagnostic HF
6	5.423 MHz		RF	Heater Tromsø	Modifier HF

NEW !

Kiruna EISCAT_3D Demonstrator Array VHF

Tromsø–Kiruna Bi-static Geometry

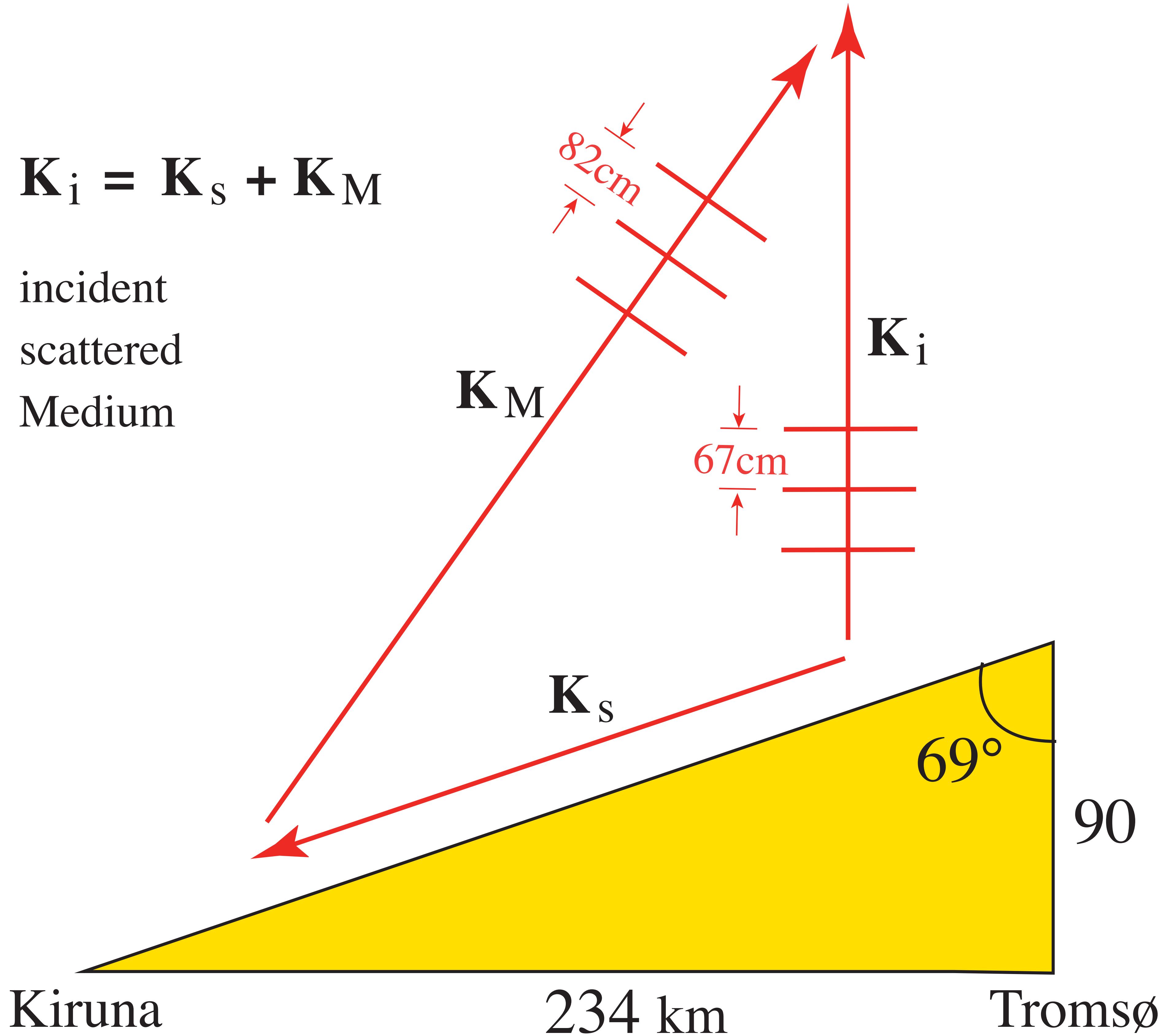

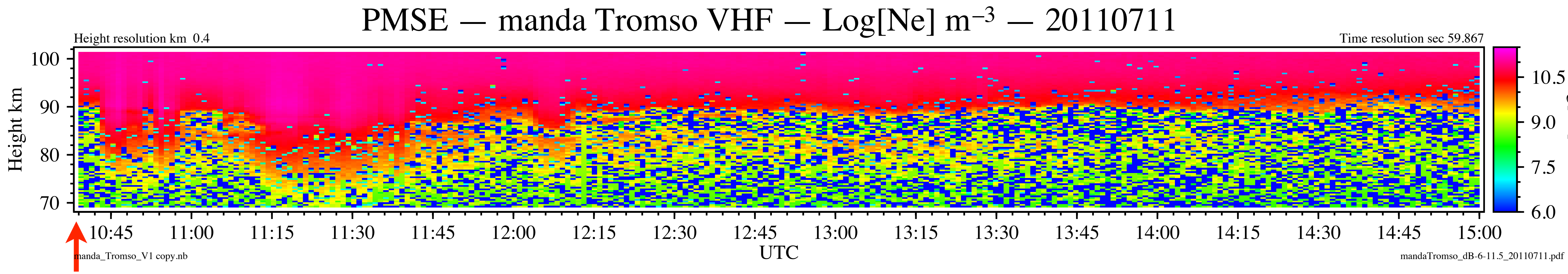
PMSE — manda Tromso VHF — Log[Ne] m−3 — 20110711
Height resolution km 0.4
Time resolution sec 59.867
Height km
100
90
80
70
10:45
11:00
11:15
11:30
11:45
12:00
12:15
12:30
12:45
13:00
13:15
13:30
13:45
14:00
14:15
14:30
14:45
15:00
UTC
10.5
9.0
7.5
6.0
Log[Ne] m−3
manda_Tromso_V1 copy.nb
mandaTromso_dB-6-11.5_20110711.pdf

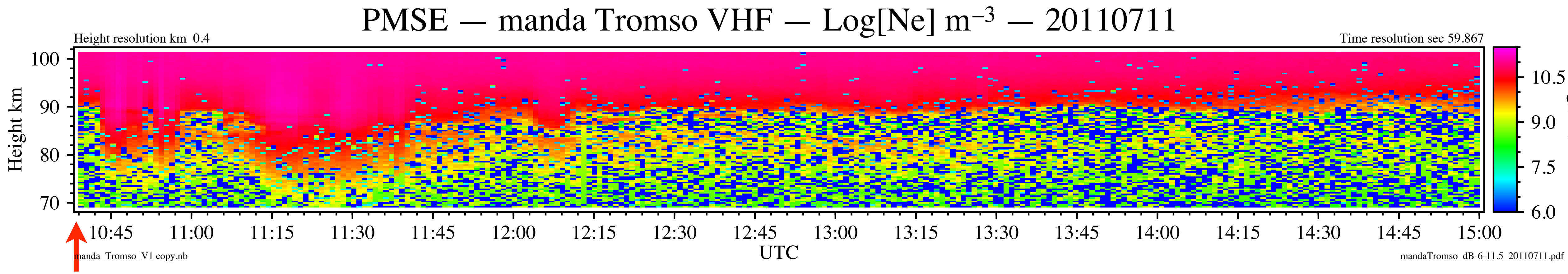
PMSE — manda Tromso VHF — Log[Ne] m^{-3} — 20110711
Height resolution km 0.4
Time resolution sec 59.867
Height km
Log[Ne] m^{-3}
UTC
manda_Tromso_V1 copy.nb
mandaTromso_dB-6-11.5_20110711.pdf

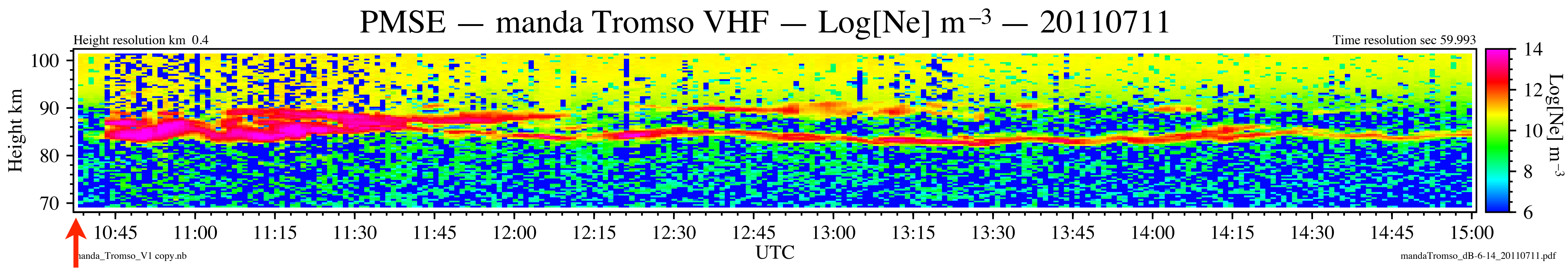
PMSE — manda Tromso VHF — Log[Ne] m^{-3} — 20110711
Height resolution km 0.4
Time resolution sec 59.993
Height km
Log[Ne] m^{-3}
UTC
manda_Tromso_V1 copy.nb
mandaTromso_dB-6-14_20110711.pdf

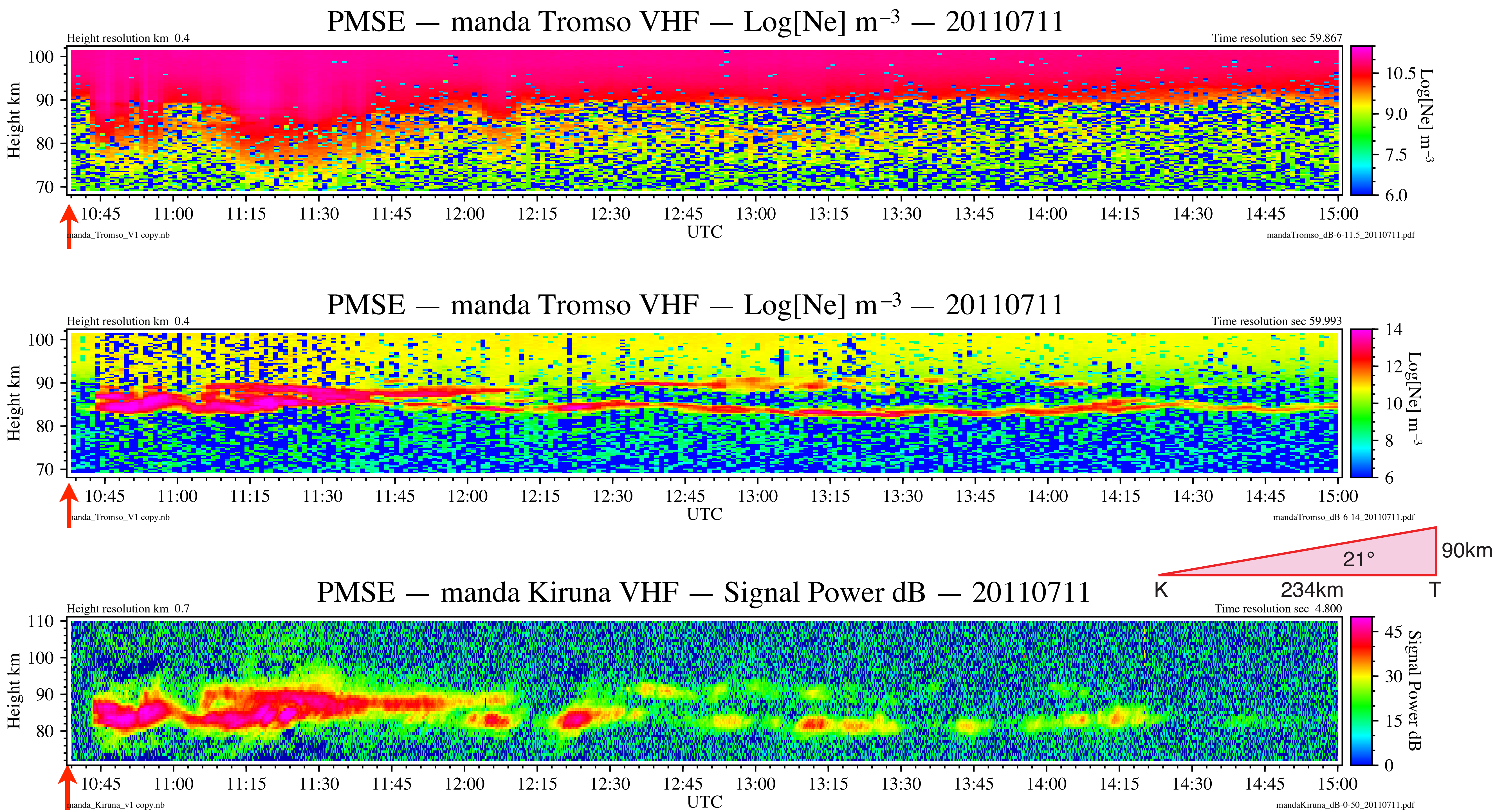

PMSE — manda Tromso VHF — Log[Ne] m⁻³ — 20110711
Height resolution km 0.4
Time resolution sec 59.867
Height km
Log[Ne] m⁻³
UTC
manda_Tromso_V1 copy.nb
mandaTromso_dB-6-11.5_20110711.pdf
PMSE — manda Tromso VHF — Log[Ne] m⁻³ — 20110711
Height resolution km 0.4
Time resolution sec 59.993
Height km
Log[Ne] m⁻³
UTC
manda_Tromso_V1 copy.nb
mandaTromso_dB-6-14_20110711.pdf
21°
90km
K
234km
T
PMSE — manda Kiruna VHF — Signal Power dB — 20110711
Height resolution km 0.7
Time resolution sec 4.800
Height km
Signal Power dB
UTC
manda_Kiruna_v1 copy.nb
mandaKiruna_dB-0-50_20110711.pdf

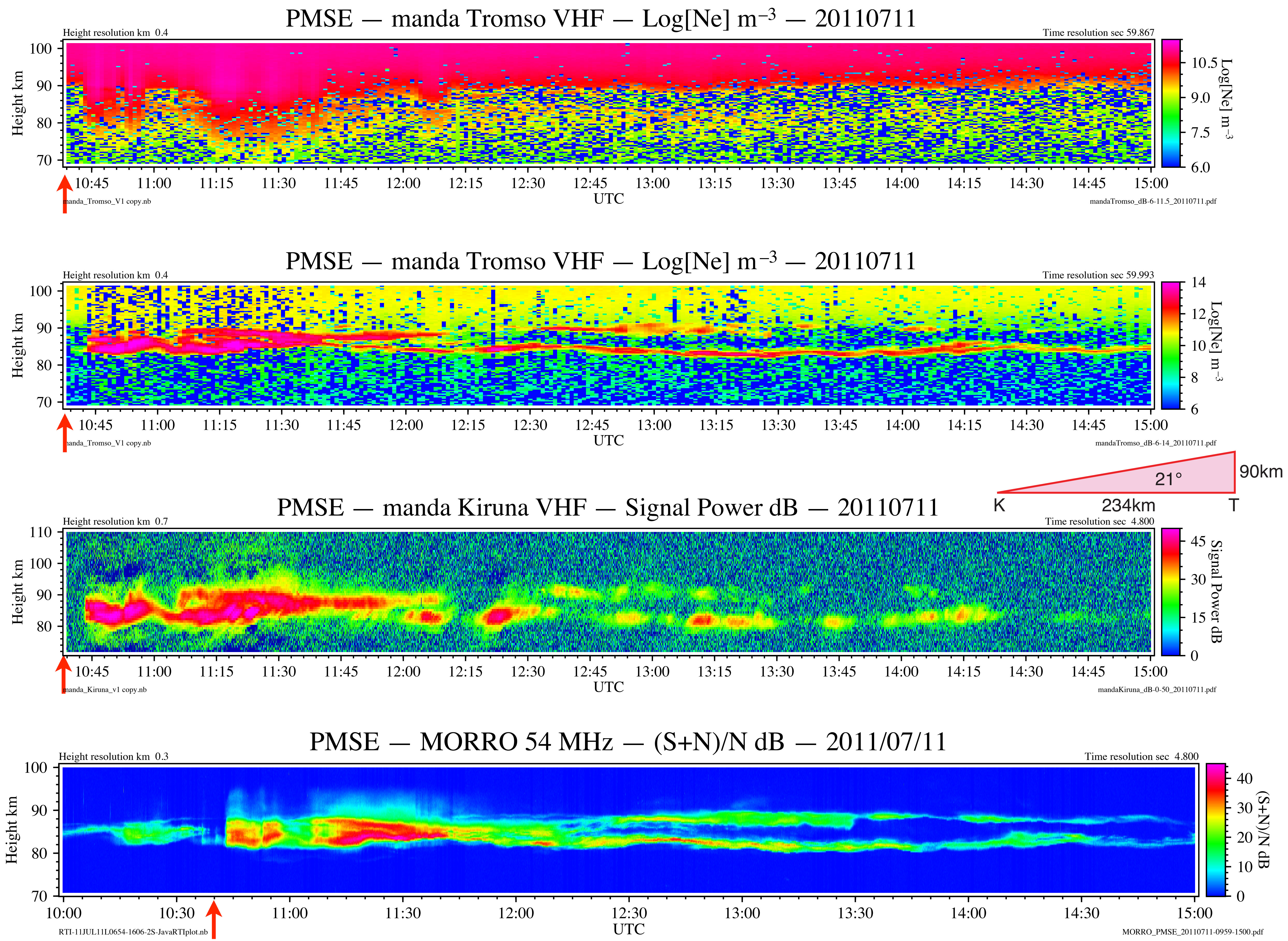
PMSE — manda Tromso VHF — Log[Ne] m^{-3} — 20110711
Height resolution km 0.4
Time resolution sec 59.867
Height km
100
90
80
70
10:45
11:00
11:15
11:30
11:45
12:00
12:15
12:30
12:45
13:00
13:15
13:30
13:45
14:00
14:15
14:30
14:45
15:00
UTC
10.5
9.0
7.5
6.0
Log[Ne] m^{-3}
manda_Tromso_V1 copy.nb
mandaTromso_dB-6-11.5_20110711.pdf
PMSE — manda Tromso VHF — Log[Ne] m^{-3} — 20110711
Height resolution km 0.4
Time resolution sec 59.993
Height km
14
12
10
8
6
Log[Ne] m^{-3}
manda_Tromso_V1 copy.nb
mandaTromso_dB-6-14_20110711.pdf
21°
90km
K
234km
T
PMSE — manda Kiruna VHF — Signal Power dB — 20110711
Height resolution km 0.7
Time resolution sec 4.800
110
45
30
15
0
Signal Power dB
manda_Kiruna_v1 copy.nb
mandaKiruna_dB-0-50_20110711.pdf
PMSE — MORRO 54 MHz — (S+N)/N dB — 2011/07/11
Height resolution km 0.3
Time resolution sec 4.800
10:00
10:30
11:00
11:30
12:00
12:30
13:00
13:30
14:00
14:30
15:00
40
30
20
10
0
(S+N)/N dB
RTI-11JUL11L0654-1606-2S-JavaRTIplot.nb
MORRO_PMSE_20110711-0959-1500.pdf

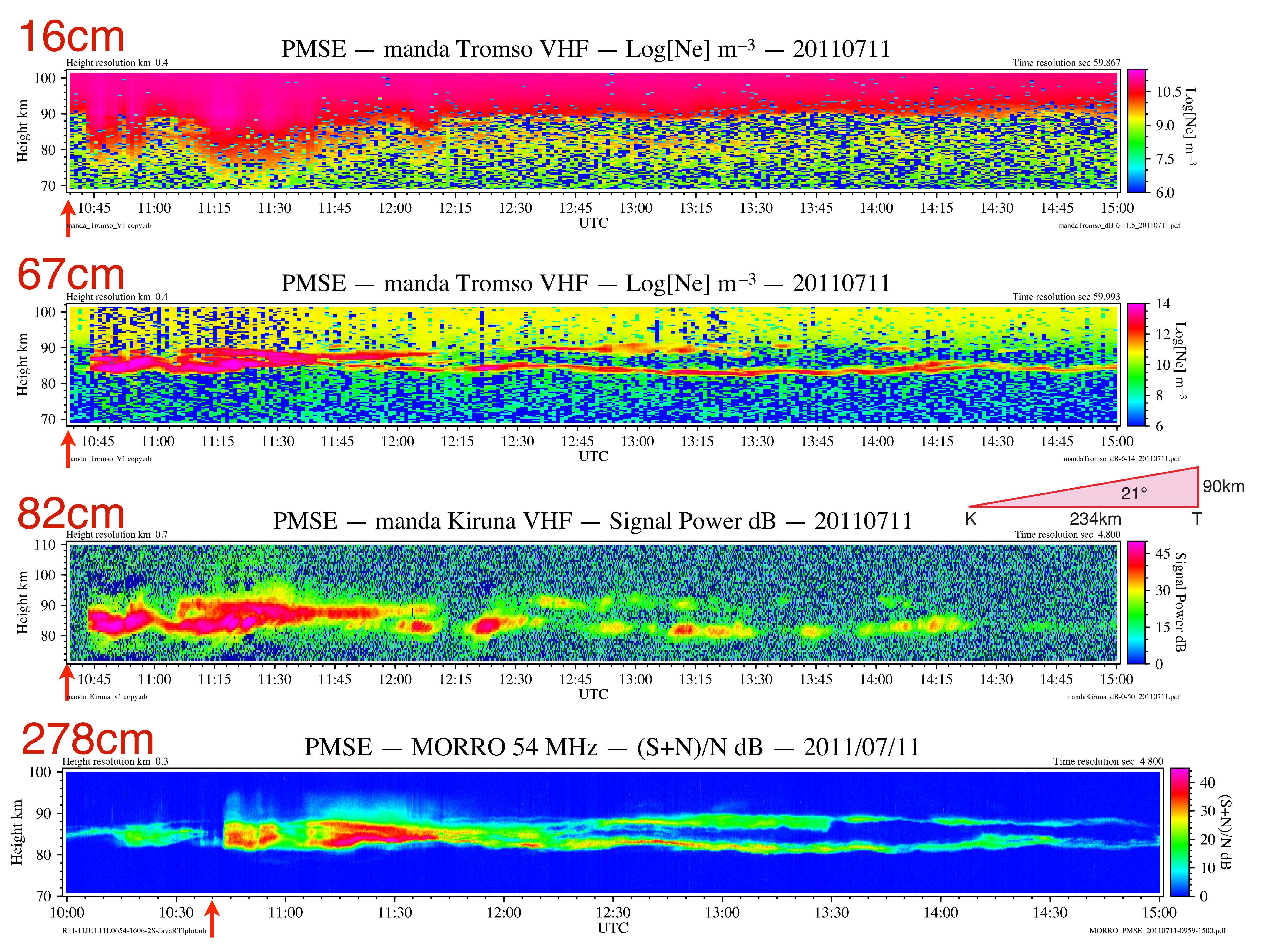
16cm
PMSE — manda Tromso VHF — Log[Ne] m−3 — 20110711
Height resolution km 0.4
Time resolution sec 59.867
Height km
Log[Ne] m−3
UTC
manda_Tromso_V1 copy.nb
mandaTromso_dB-6-11.5_20110711.pdf
67cm
PMSE — manda Tromso VHF — Log[Ne] m−3 — 20110711
Height resolution km 0.4
Time resolution sec 59.993
Height km
Log[Ne] m−3
UTC
manda_Tromso_V1 copy.nb
mandaTromso_dB-6-14_20110711.pdf
21°
90km
K
234km
T
82cm
PMSE — manda Kiruna VHF — Signal Power dB — 20110711
Height resolution km 0.7
Time resolution sec 4.800
Height km
Signal Power dB
UTC
manda_Kiruna_v1 copy.nb
mandaKiruna_dB-0-50_20110711.pdf
278cm
PMSE — MORRO 54 MHz — (S+N)/N dB — 2011/07/11
Height resolution km 0.3
Time resolution sec 4.800
Height km
(S+N)/N dB
UTC
RTI-11JUL11L0654-1606-2S-JavaRTIplot.nb
MORRO_PMSE_20110711-0959-1500.pdf

19m

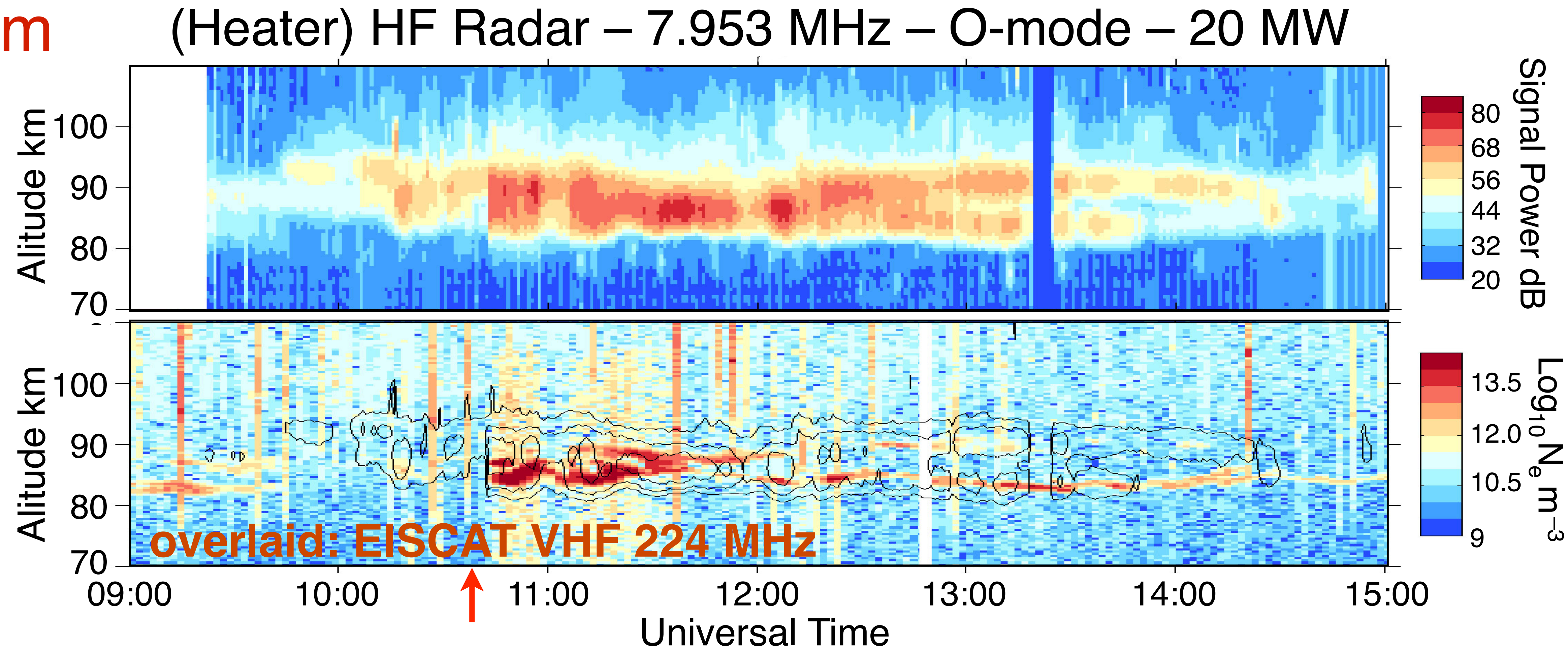
(Heater) HF Radar – 7.953 MHz – O-mode – 20 MW
Altitude km
100
90
80
70
Signal Power dB
80
68
56
44
32
20
Altitude km
100
90
80
70
overlaid: EISCAT VHF 224 MHz
Log10 Ne m−3
13.5
12.0
10.5
9
09:00
10:00
11:00
12:00
13:00
14:00
15:00
Universal Time

67cm

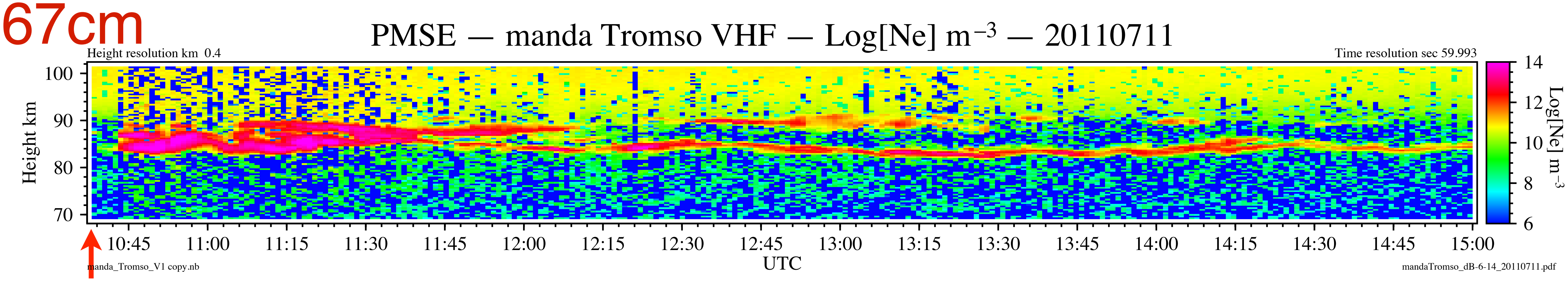
PMSE — manda Tromso VHF — Log[Ne] m−3 — 20110711
Height resolution km 0.4
Time resolution sec 59.993
Height km
100
90
80
70
Log[Ne] m−3
14
12
10
8
6
10:45
11:00
11:15
11:30
11:45
12:00
12:15
12:30
12:45
13:00
13:15
13:30
13:45
14:00
14:15
14:30
14:45
15:00
UTC
manda_Tromso_V1 copy.nb
mandaTromso_dB-6-14_20110711.pdf

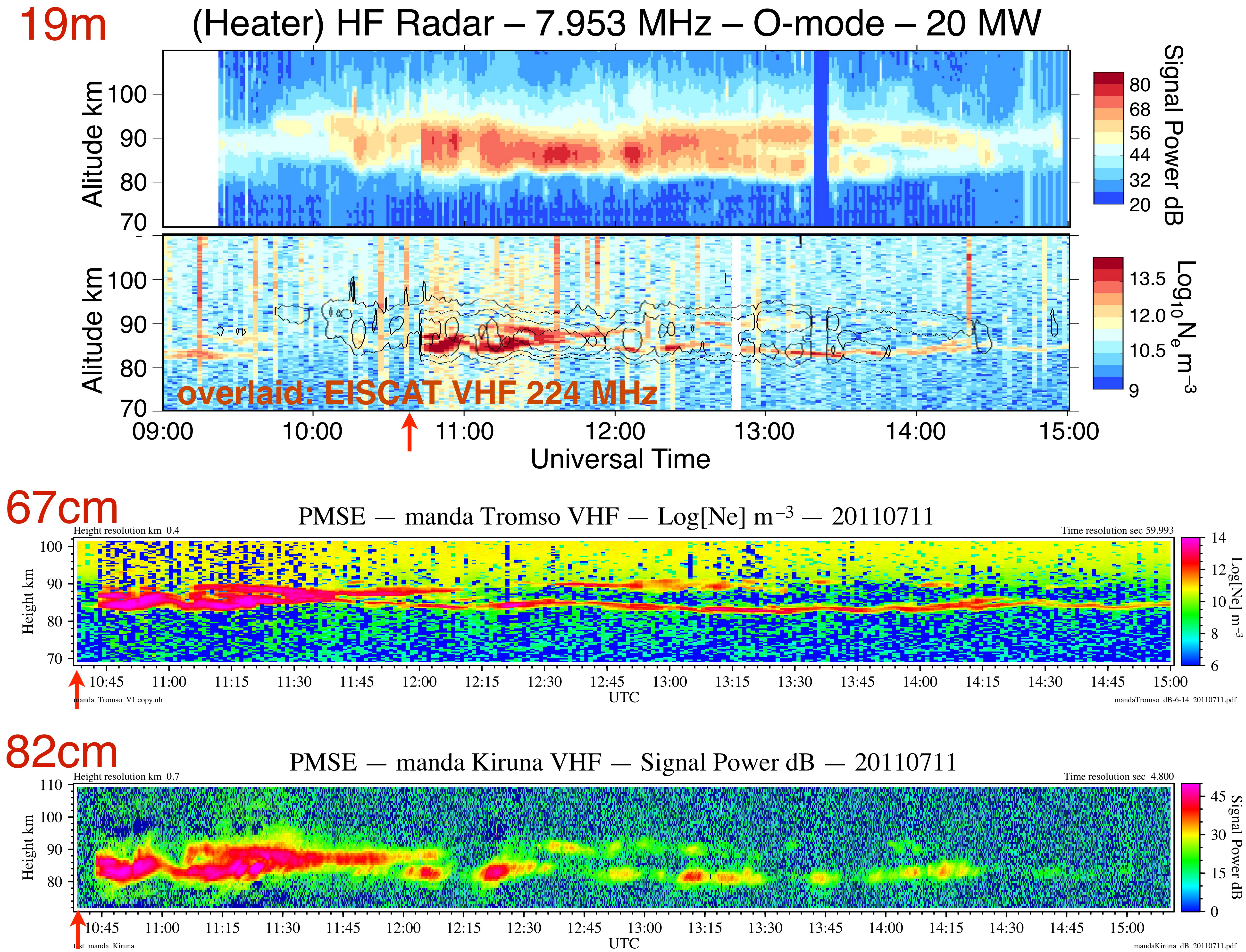

19m
(Heater) HF Radar – 7.953 MHz – O-mode – 20 MW
Altitude km
Signal Power dB
80
68
56
44
32
20
Log10 Ne m−3
13.5
12.0
10.5
9
overlaid: EISCAT VHF 224 MHz
09:00
10:00
11:00
12:00
13:00
14:00
15:00
Universal Time
67cm
PMSE — manda Tromso VHF — Log[Ne] m−3 — 20110711
Height resolution km 0.4
Time resolution sec 59.993
Height km
Log[Ne] m−3
UTC
manda_Tromso_V1 copy.nb
mandaTromso_dB-6-14_20110711.pdf
82cm
PMSE — manda Kiruna VHF — Signal Power dB — 20110711
Height resolution km 0.7
Time resolution sec 4.800
Height km
Signal Power dB
UTC
mandaKiruna_dB_20110711.pdf

Tromsø–Kiruna Bi-static Geometry again

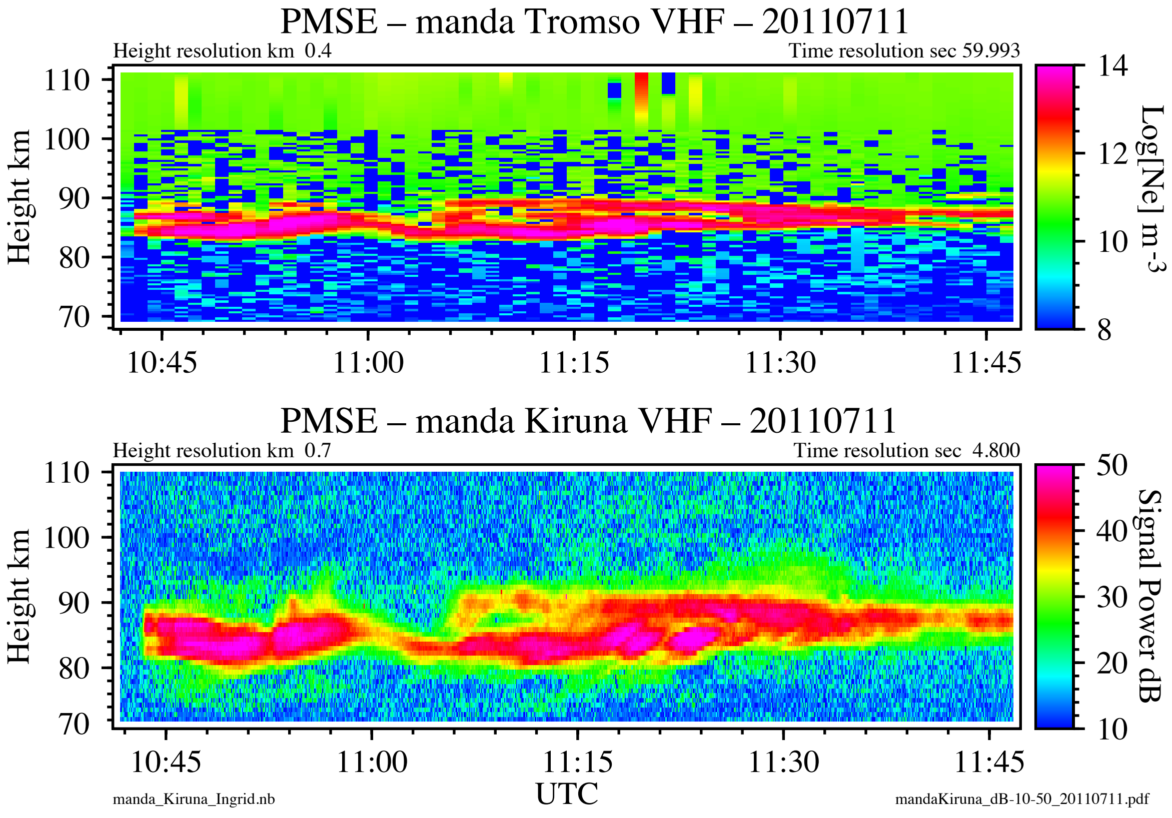

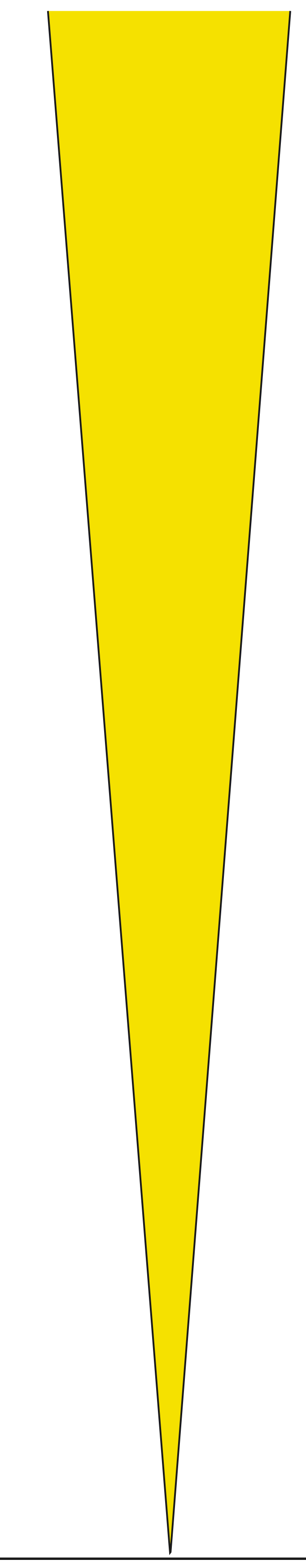

Tromsø–Kiruna Bi-static Geometry again

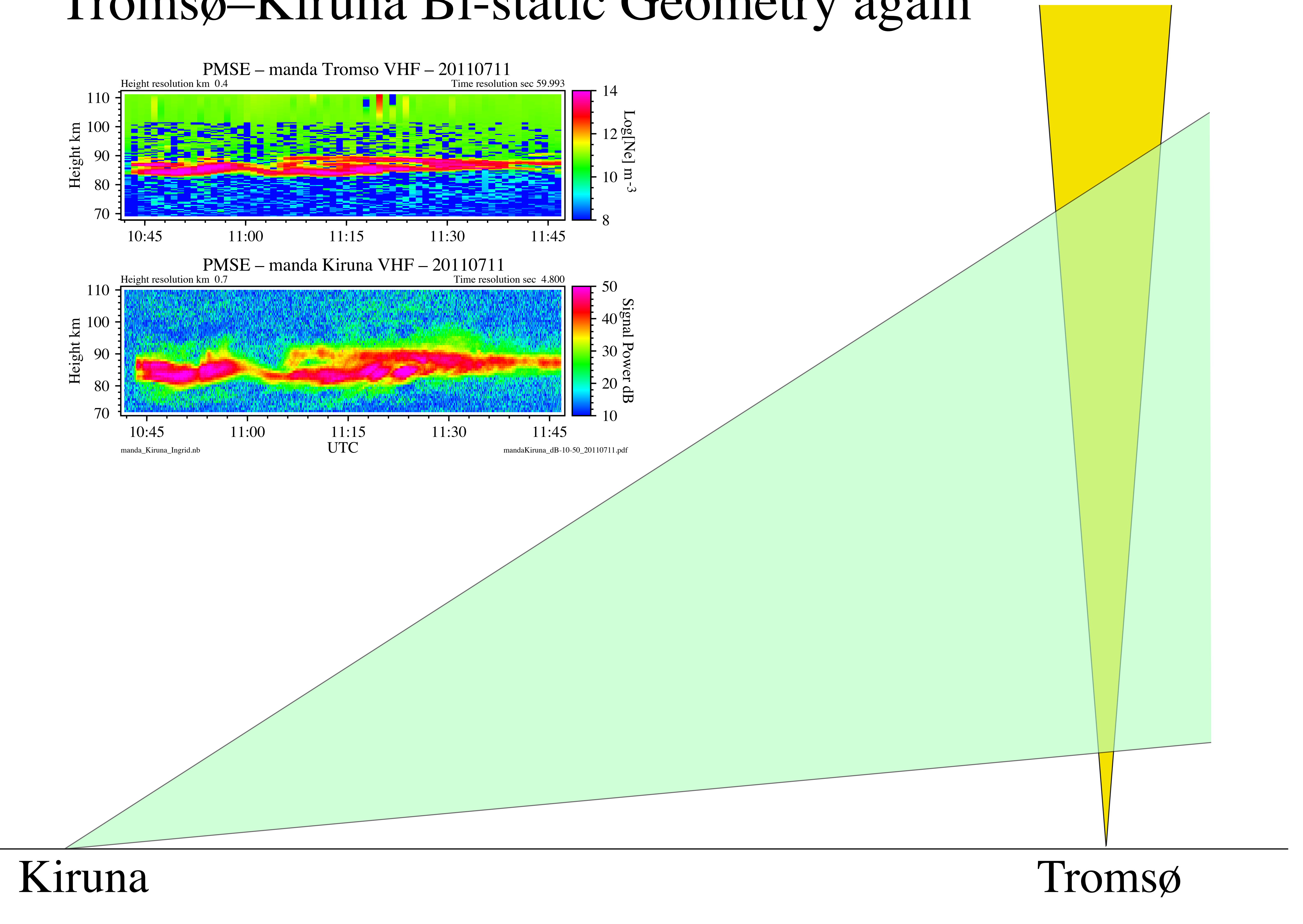

Tromsø–Kiruna Bi-static Geometry again

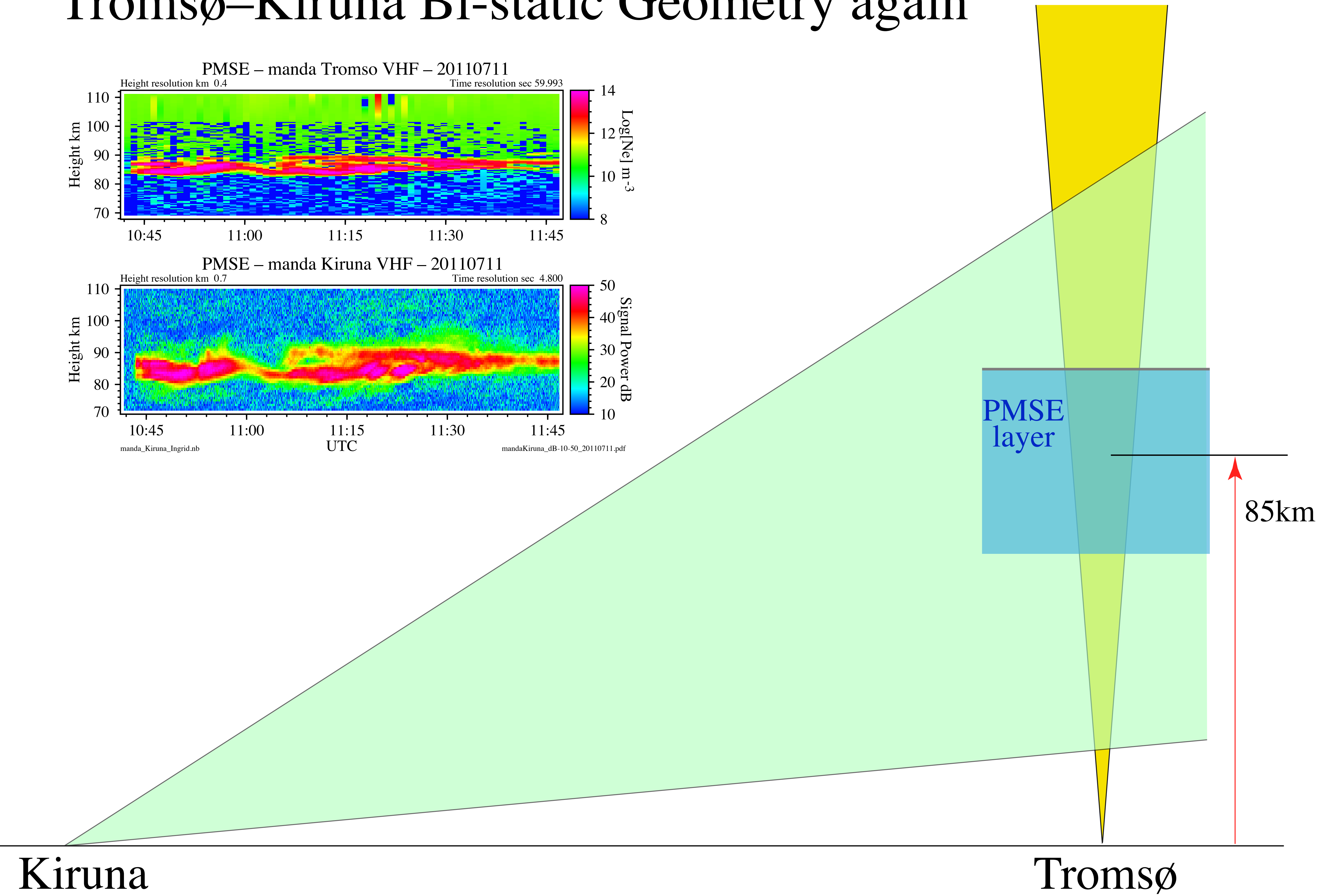

Tromsø–Kiruna Bi-static Geometry again

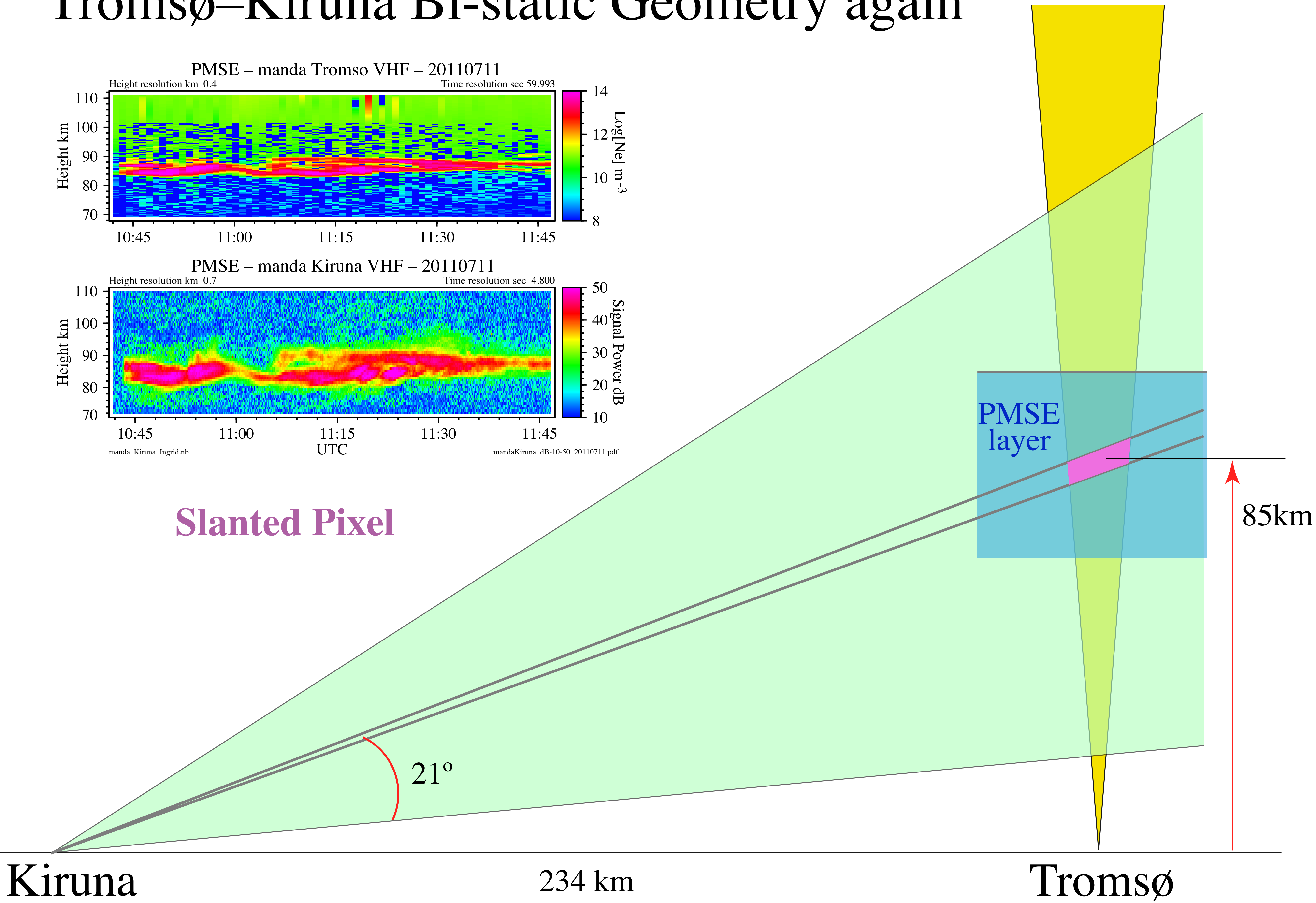

Aspect Sensitivity of PMSE
Anisotropic (specular) or Isotropic Scatterers ?

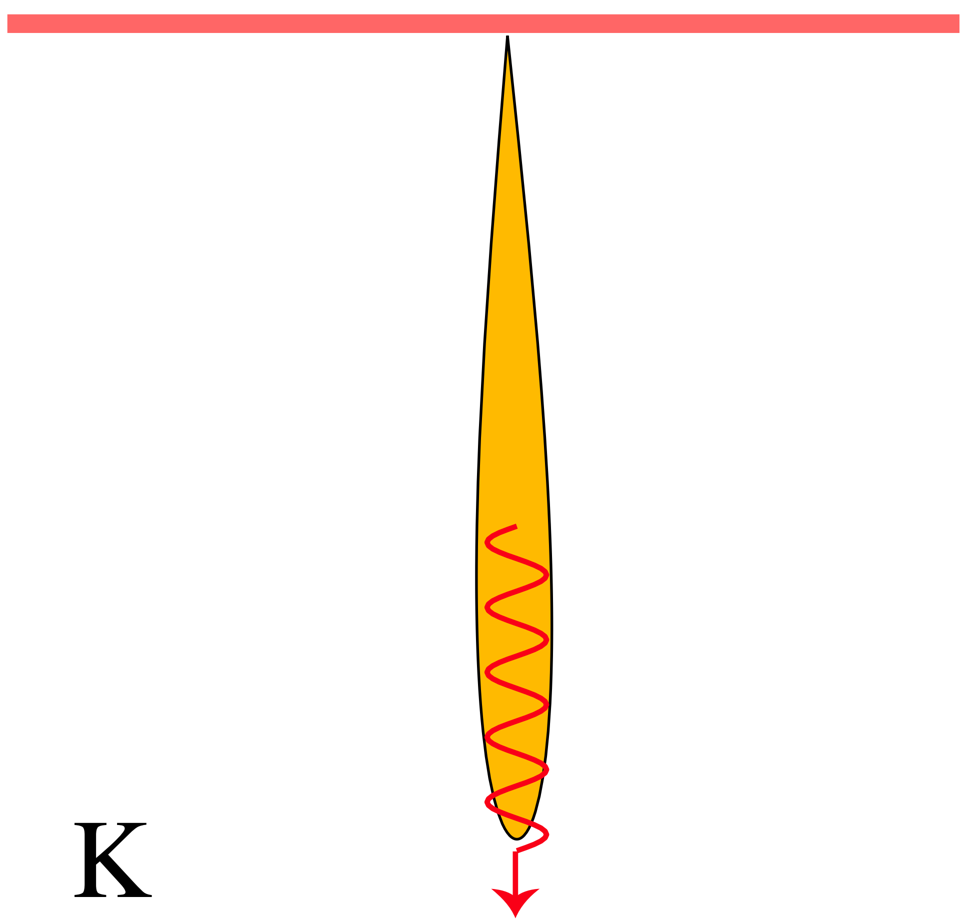

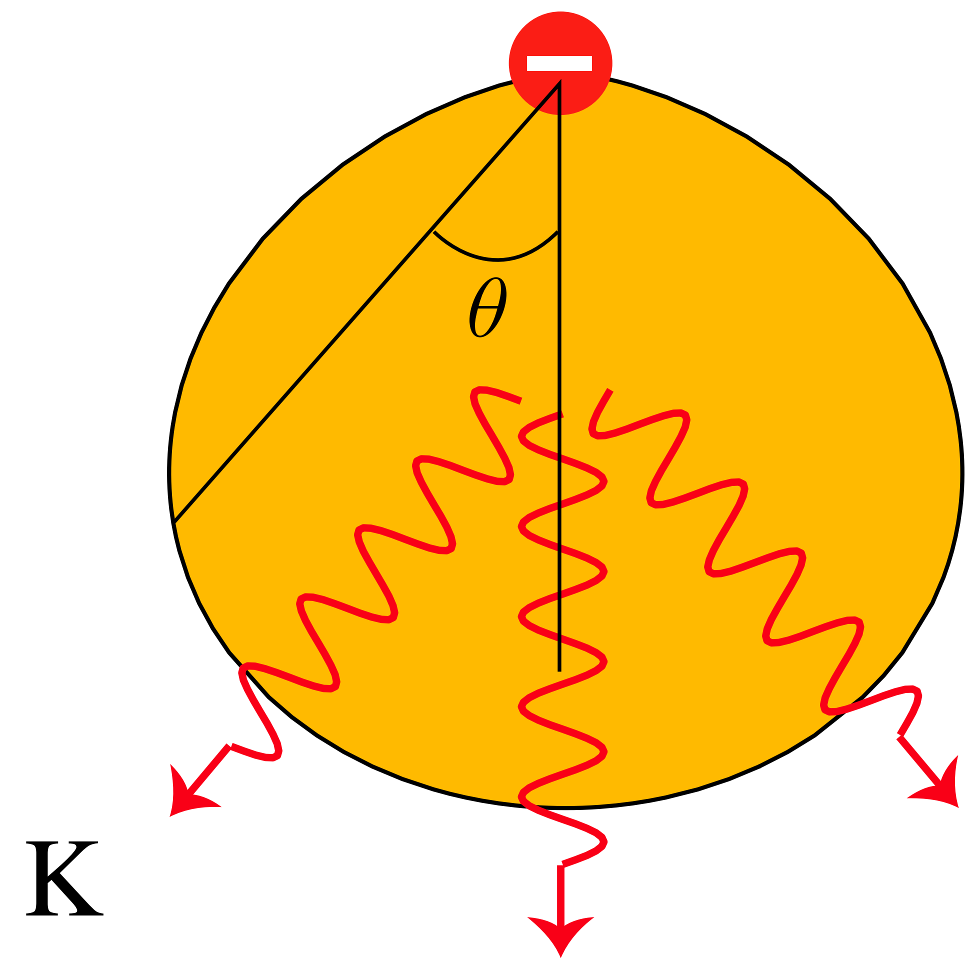

$$\mathcal{P} \sim \mathrm{e}^{\theta^2/2\theta_o^2}$$

$$\cos^2\theta$$

Aspect Sensitivity of PMSE

Anisotropic (specular) or Isotropic Scatterers ?

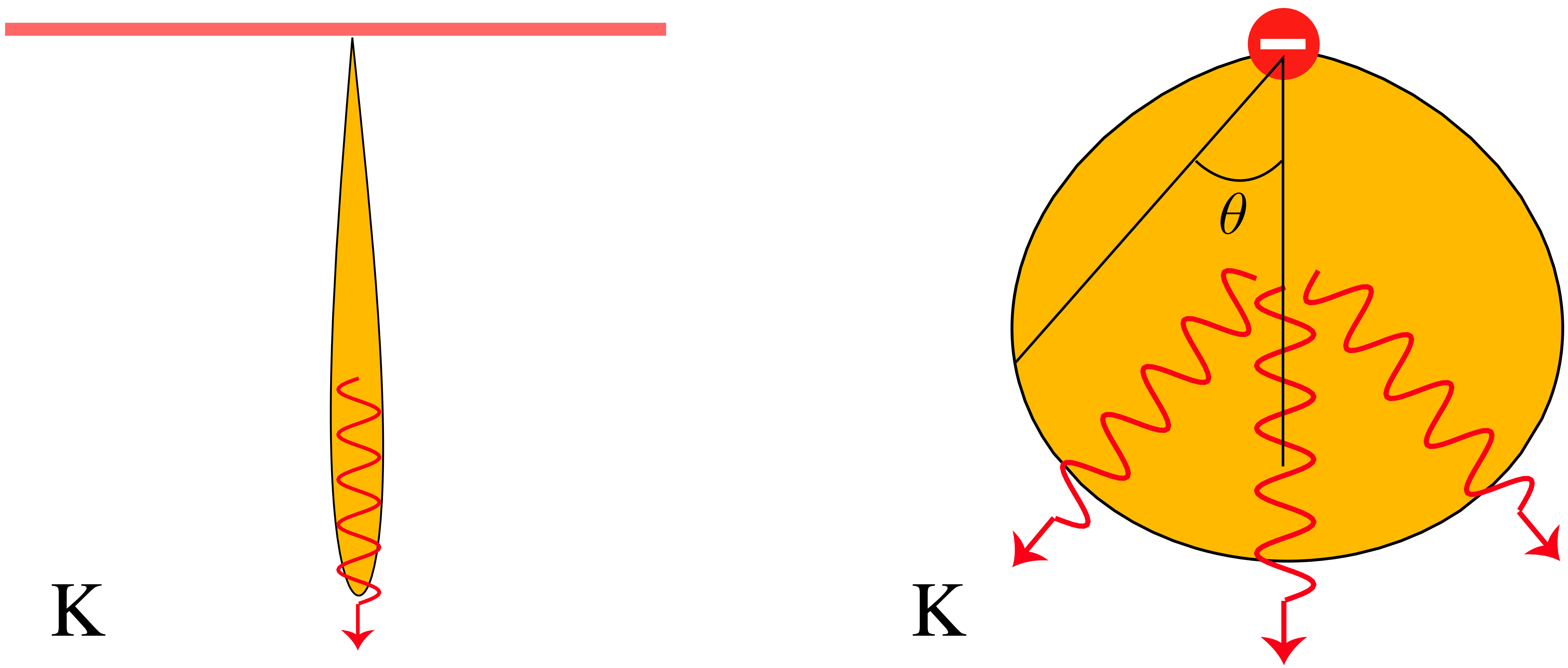

$$\mathcal{P} \sim \mathrm{e}^{\theta^2/2\theta_\mathrm{o}^2} \qquad\qquad \cos^2\theta$$

Ans: 11 July 2011, Isotropic nearly continuously, $\theta = 69^\circ$

PMWE
MORRO

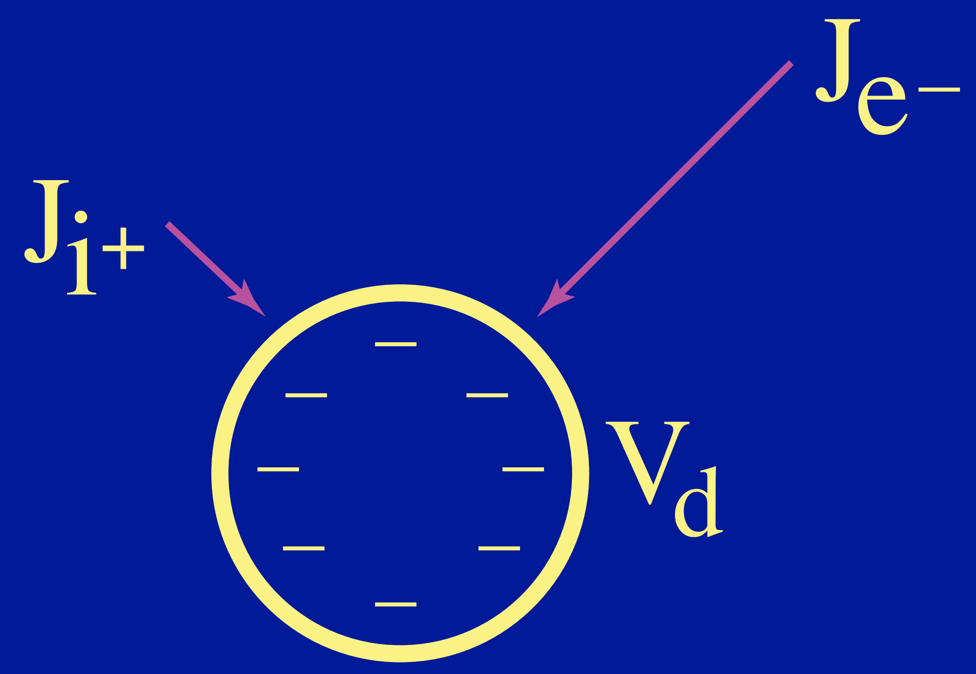

The mesosphere has free electrons and ions: thermal current equilibrium demands negative charge on the dust particles

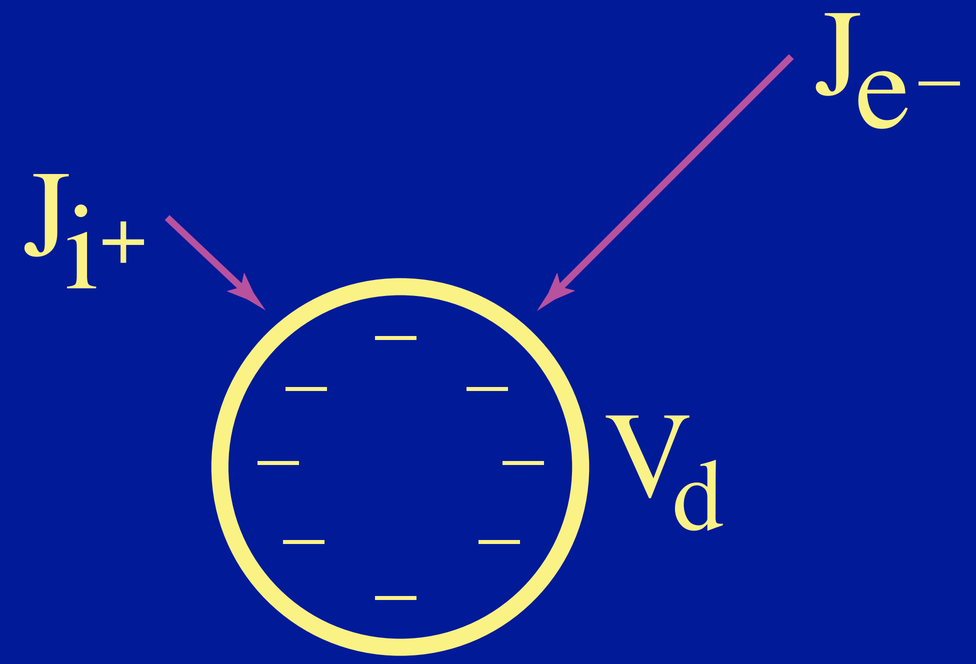

$$J = n\, v_{thermal} \qquad \begin{matrix} v_e \gg v_i \\ n_e = n_i \end{matrix} \qquad J_e \gg J_i$$

The mesosphere has free electrons and ions: thermal current equilibrium demands negative charge on the dust particles

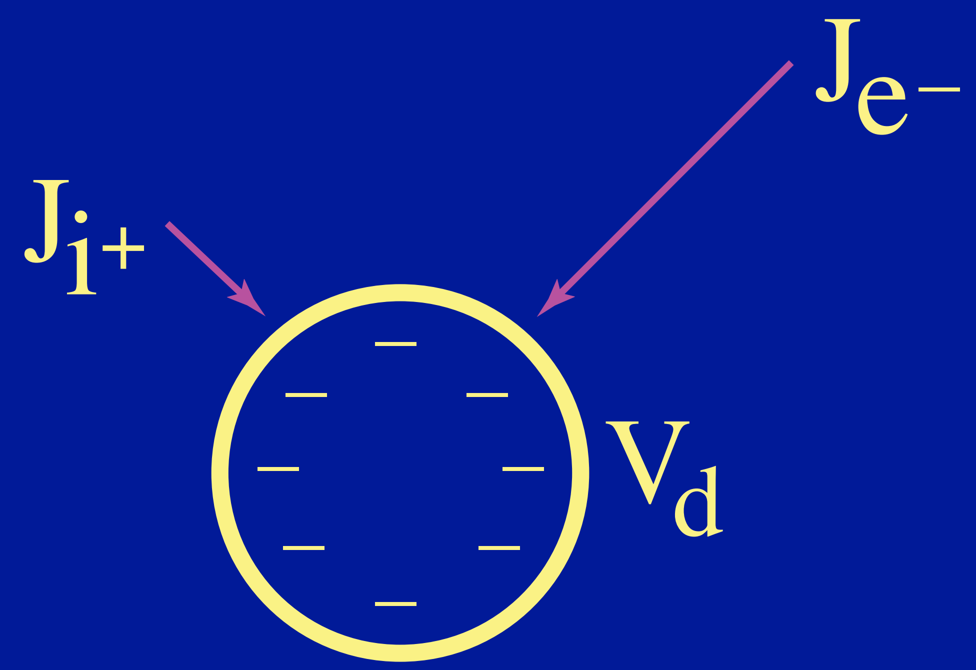

$$J = n\, v_{thermal} \qquad \begin{array}{c} v_e \gg v_i \\ n_e = n_i \end{array} \qquad J_e \gg J_i$$

$$J_{i+} + J_{e-} = 0 \;\Rightarrow\; V_d \neq 0$$

The mesosphere has free electrons and ions: thermal current equilibrium demands negative charge on the dust particles

Polar Mesospheric Winter Echoes (Ove)

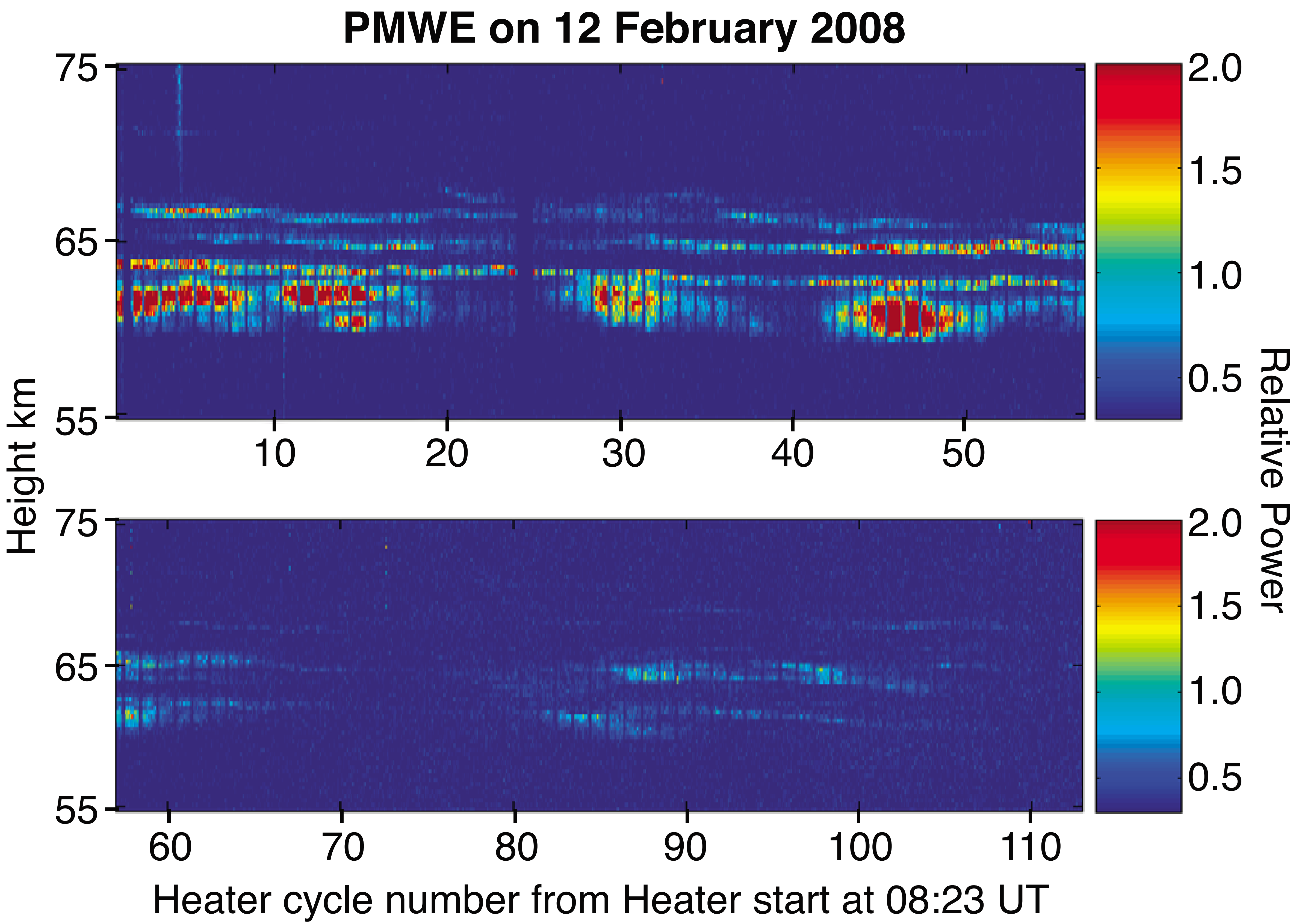

Polar Mesospheric Winter Echoes (Ove)

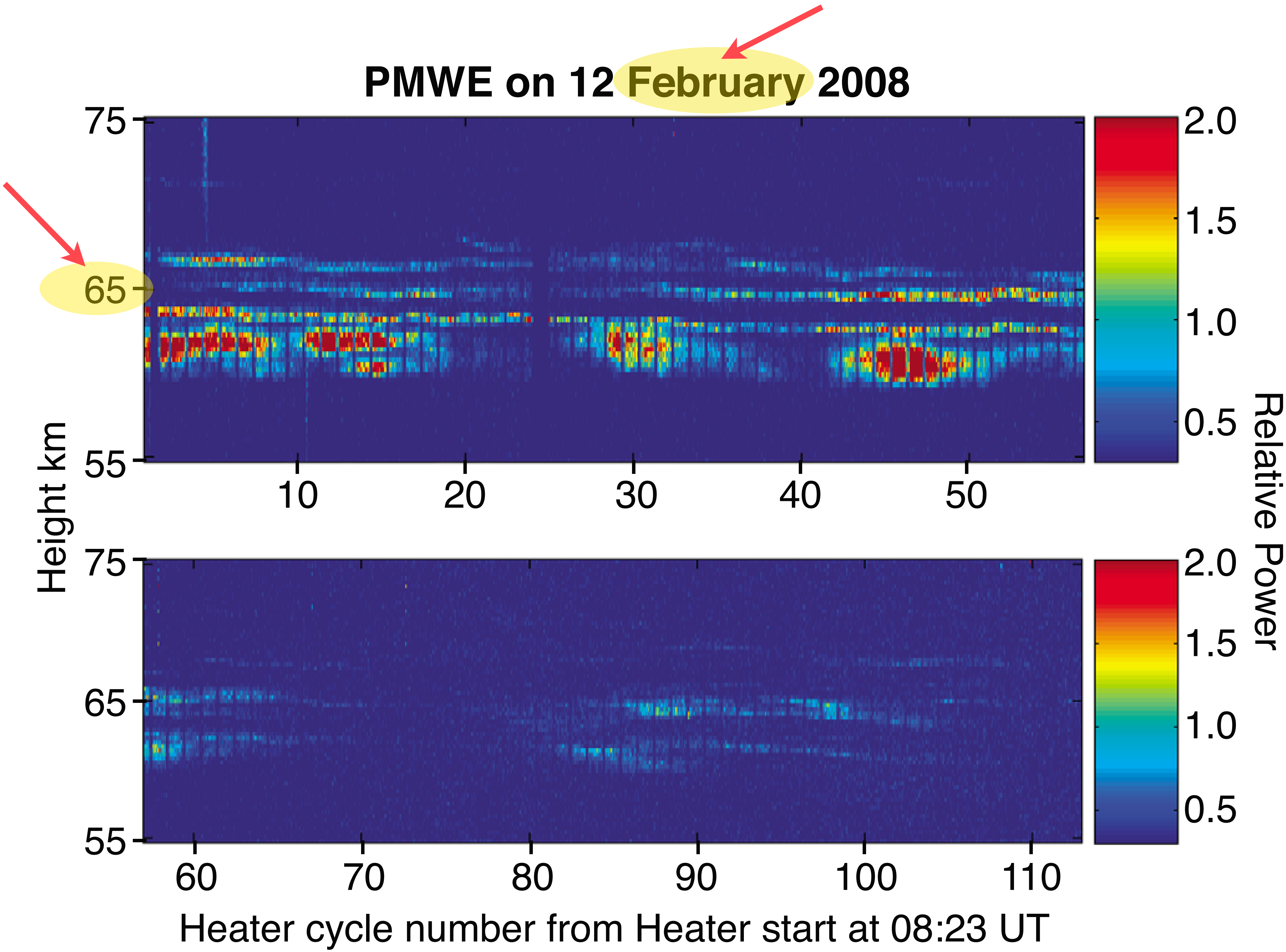

PMWE overshoot has an exponential decay with a time constant of ~62 seconds

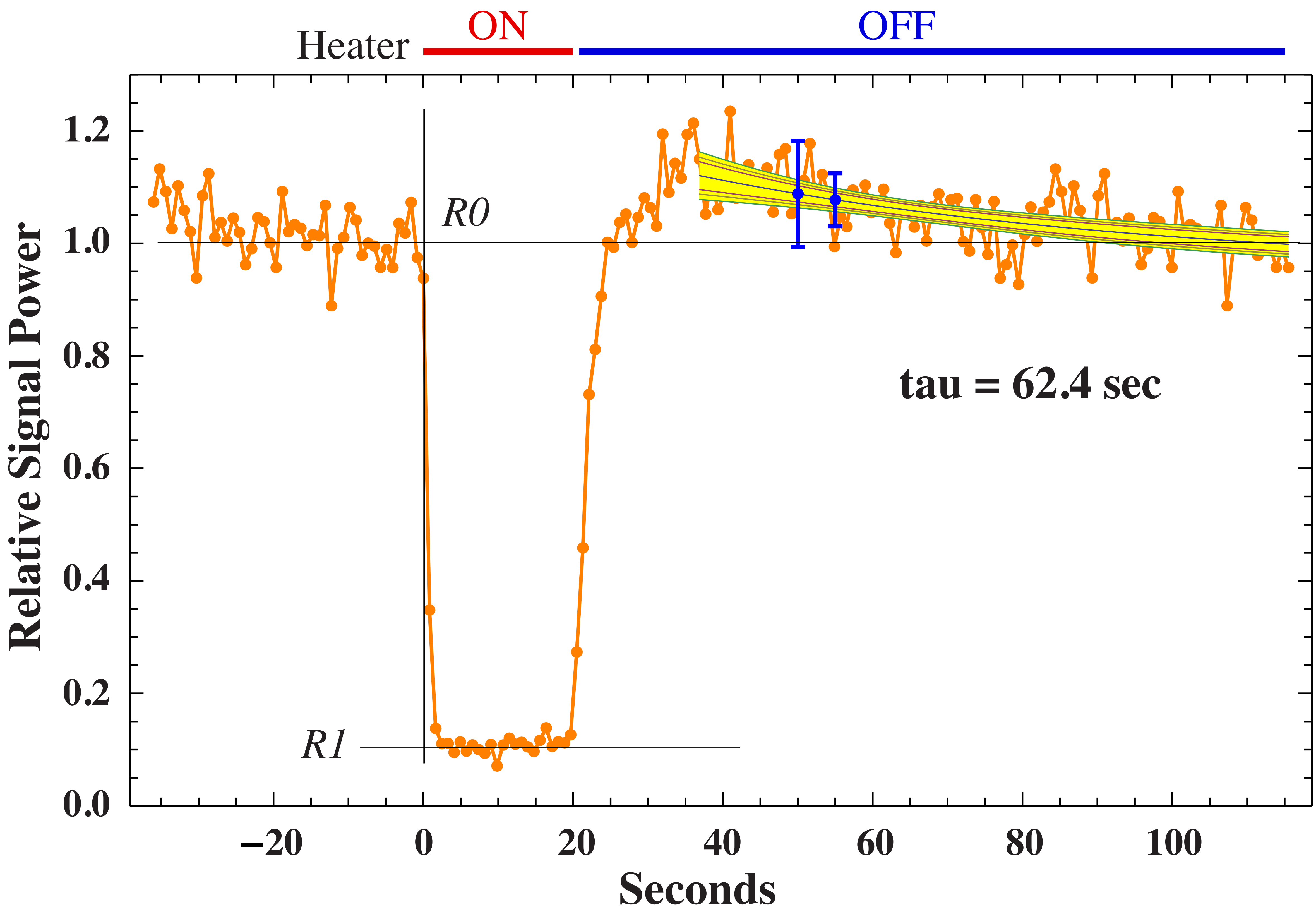

PMWE by MORRO

The observed overshoot implies a role of charged aerosols, most likely nanometre-size meteoritic smoke

PMWE by MORRO

The observed overshoot implies a role of charged aerosols, most likely nanometre-size meteoritic smoke

PMWE overshoot decays exponentially with a time constant of ~62 seconds

PMWE by MORRO

The observed overshoot implies a role of charged aerosols, most likely nanometre-size meteoritic smoke

PMWE overshoot decays exponentially with a time constant of ~62 seconds

Implying that the most likely discharge mechanism is photo-detachment as opposed to ion-attachment

PMWE by MORRO

The observed overshoot implies a role of charged aerosols, most likely nanometre-size meteoritic smoke

---

PMWE overshoot decays exponentially with a time constant of ~62 seconds

---

Implying that the most likely discharge mechanism is photo-detachment as opposed to ion-attachment

---

O. Havnes, C. La Hoz, M.T. Rietveld, M. Kassa, G. Baroni and A. Biebricher (2011), Dust Charging and density conditions deduced from observations of PMWE modulated by artificial electron heating; JGR, submitted for publication.

Aperture Synthesis Imaging Radar (Vasyl)

ASIR + EASI ESR

VLBI – Very Long Baseline Interferometry

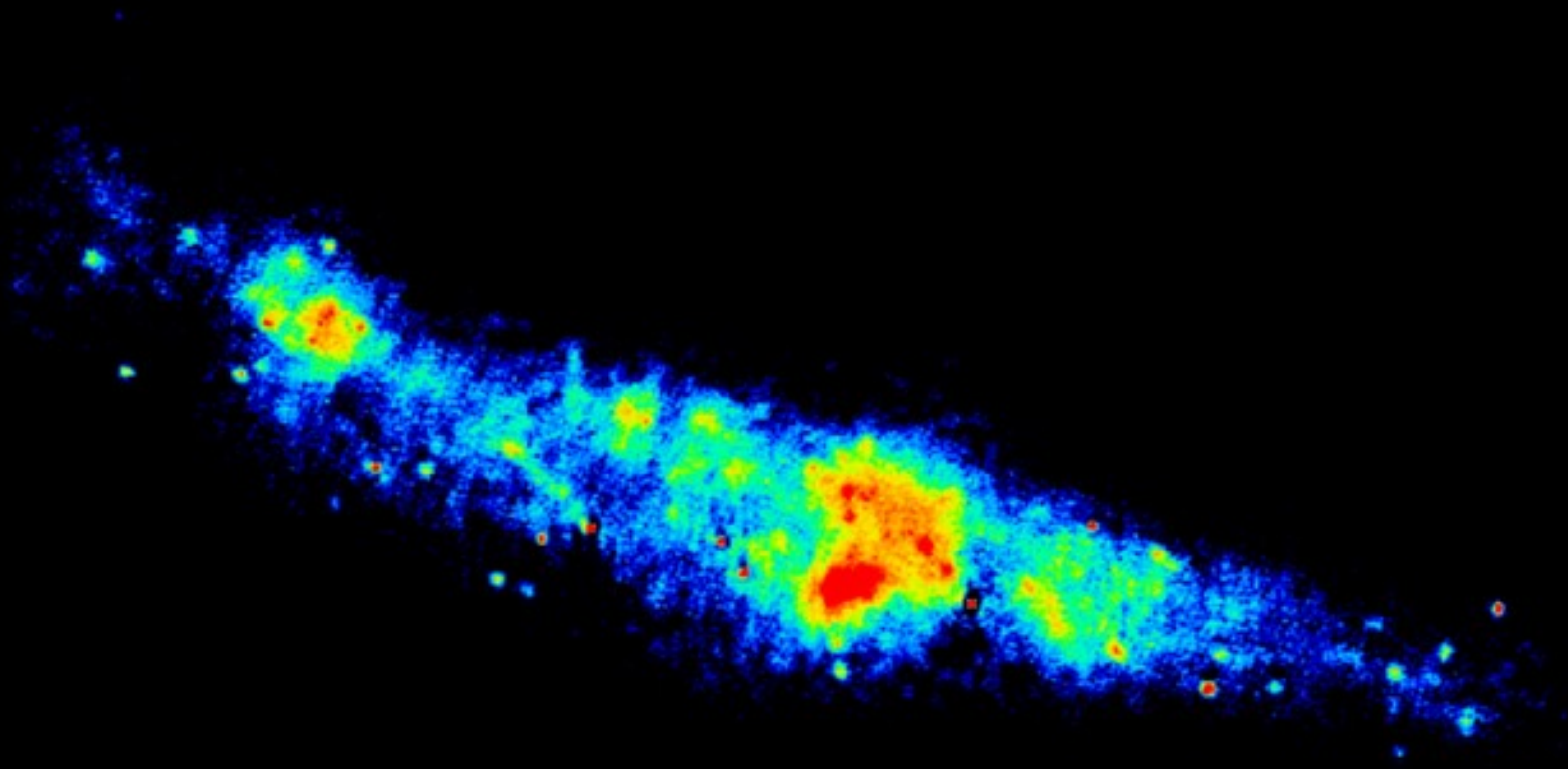

Starburst Galaxy M82: 12 million lightyears away

The Visibility is the spatial autocorrelation function of the incident radiation field at the aperture plane.

Aperture Synthesis Imaging Radar ASIR

How it works 1

Aperture Synthesis Imaging Radar ASIR

How it works 1

Brightness at the source	$B_\omega(\mathbf{s}) = \langle |\mathcal{E}_\omega(\mathbf{s})|^2 \rangle$

Aperture Synthesis Imaging Radar ASIR

How it works 1

Brightness at the source	$B_\omega(\mathbf{s}) = \langle |\mathcal{E}_\omega(\mathbf{s})|^2 \rangle$
Follows from Huygens principle	$V_\omega(\mathbf{r}_1, \mathbf{r}_2) = \int B_\omega(\mathbf{s}) \exp[-i\,\omega\,\mathbf{s}\cdot(\mathbf{r}_1 - \mathbf{r}_2)/c]\,\mathrm{d}\Omega$

Aperture Synthesis Imaging Radar ASIR

How it works 1

Brightness at the source	$B_\omega(\mathbf{s}) = \langle|\mathcal{E}_\omega(\mathbf{s})|^2\rangle$
Follows from Huygens principle	$V_\omega(\mathbf{r}_1, \mathbf{r}_2) = \int B_\omega(\mathbf{s}) \exp[-i\,\omega\,\mathbf{s}\cdot(\mathbf{r}_1 - \mathbf{r}_2)/c]\,\mathrm{d}\Omega$
Visibility at the Aperture Plane	$V_\omega(u, v) = \iint \frac{B_\omega(l, m)}{\sqrt{1 - l^2 - m^2}} e^{-2\pi i(ul+vm)} dl\, dm$

Aperture Synthesis Imaging Radar ASIR

How it works 1

Brightness at the source	$B_\omega(\mathbf{s}) = \langle \lvert \mathcal{E}_\omega(\mathbf{s}) \rvert^2 \rangle$
Follows from Huygens principle	$V_\omega(\mathbf{r}_1, \mathbf{r}_2) = \int B_\omega(\mathbf{s}) \exp[-i\,\omega\,\mathbf{s} \cdot (\mathbf{r}_1 - \mathbf{r}_2)/c]\,\mathrm{d}\Omega$
Visibility at the Aperture Plane	$V_\omega(u,v) = \iint \frac{B_\omega(l,m)}{\sqrt{1-l^2-m^2}} e^{-2\pi i(ul+vm)} dl\,dm$
Brightness–Visibility 2-D *Fourier* pair	$\frac{B_\omega(l,m)}{\sqrt{1-l^2-m^2}} = \iint V_\omega(u,v) e^{2\pi i(ul+vm)} du\,dv$

Van Cittert-Zernik theorem

Brightness in **s**-space
B(s)

$$\mathbf{s} = (l, m, n)$$

$$l = \cos(\alpha)$$

$$m = \cos(\beta)$$

$$n = \cos(\gamma) = \sqrt{1 - l^2 - m^2}$$

s are direction cosines:
Brightness Distribution is an Angular Spectrum.

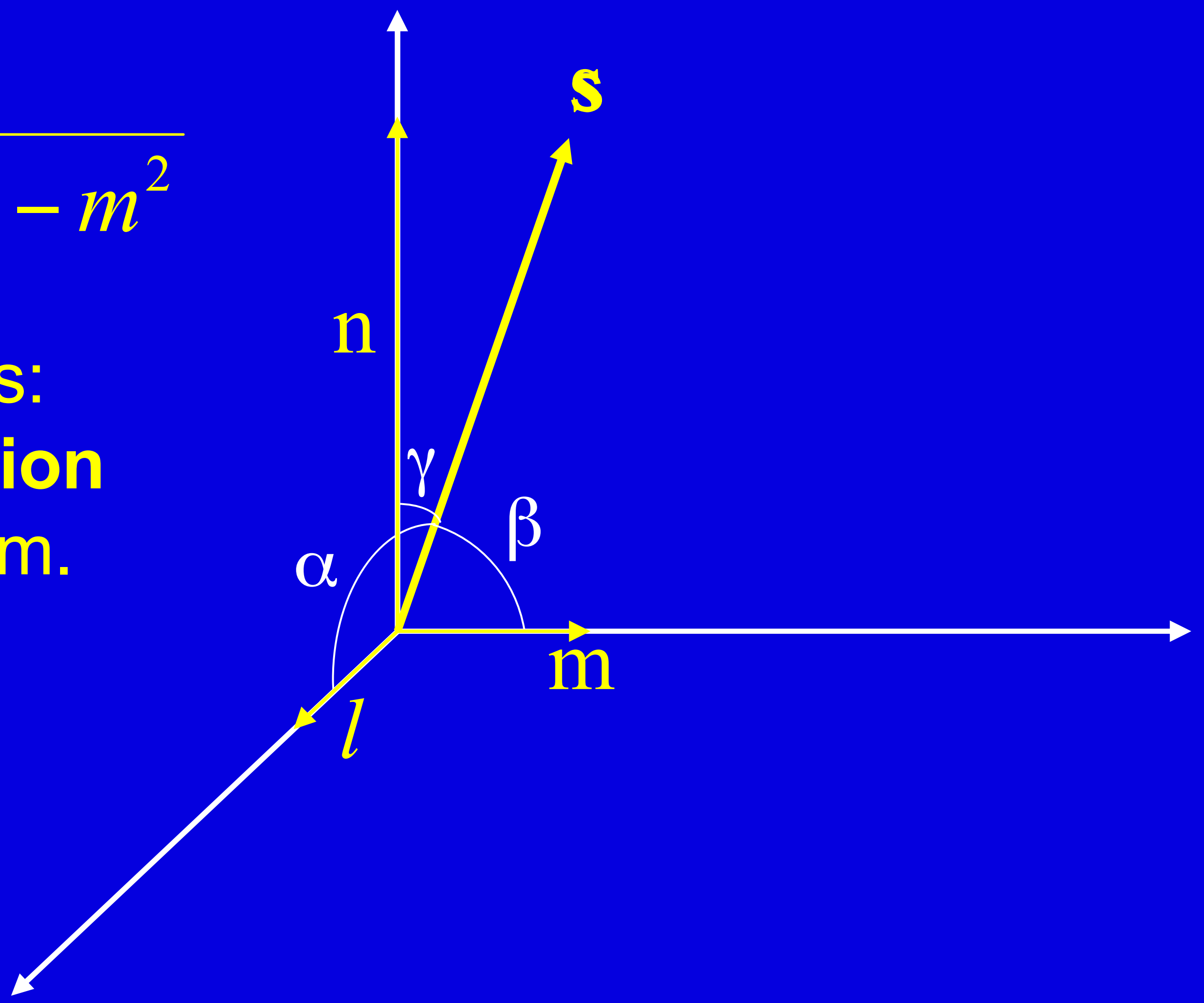

Brightness in s-space and Visibility in b-Space

B(s)

$$\mathbf{s} = (l, m, n)$$

$$l = \cos(\alpha)$$

$$m = \cos(\beta)$$

$$n = \cos(\gamma) = \sqrt{1 - l^2 - m^2}$$

s are direction cosines: **Brightness Distribution** is an Angular Spectrum.

V(b)

$$\mathbf{b} = (u, v, w)$$

b is the baseline of pairs of antennas: **Visibility Function** is the spatial Autocorrelation of the E-field distribution on the plane of measurement.

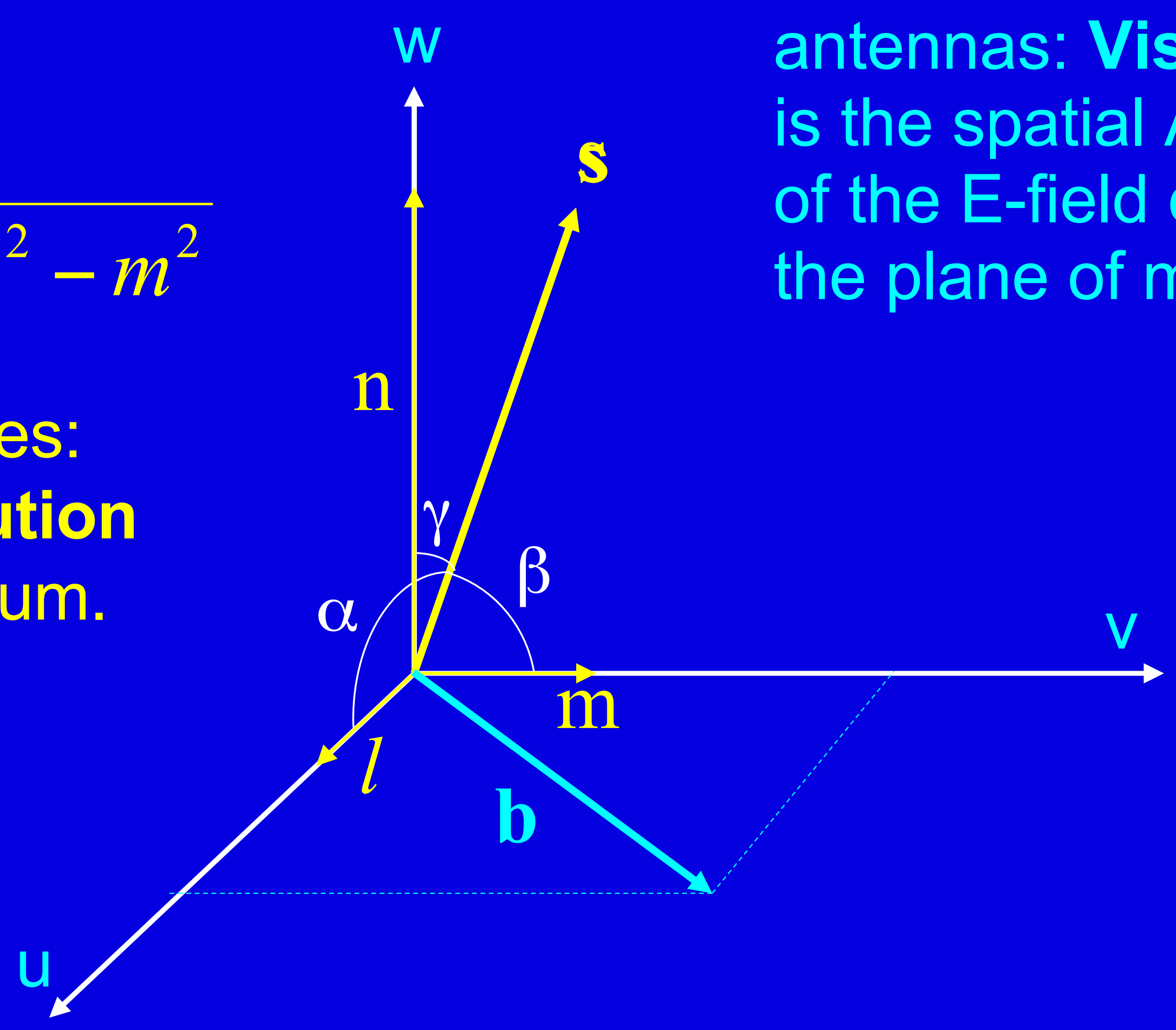

Brightness in s-space and Visibility in b-Space

B(s)

$$\mathbf{s} = (l, m, n)$$

$$l = \cos(\alpha)$$

$$m = \cos(\beta)$$

$$n = \cos(\gamma) = \sqrt{1 - l^2 - m^2}$$

s are direction cosines: **Brightness Distribution** is an Angular Spectrum.

V(b)

$$\mathbf{b} = (u, v, w)$$

b is the baseline of pairs of antennas: **Visibility Function** is the spatial Autocorrelation of the E-field distribution on the plane of measurement.

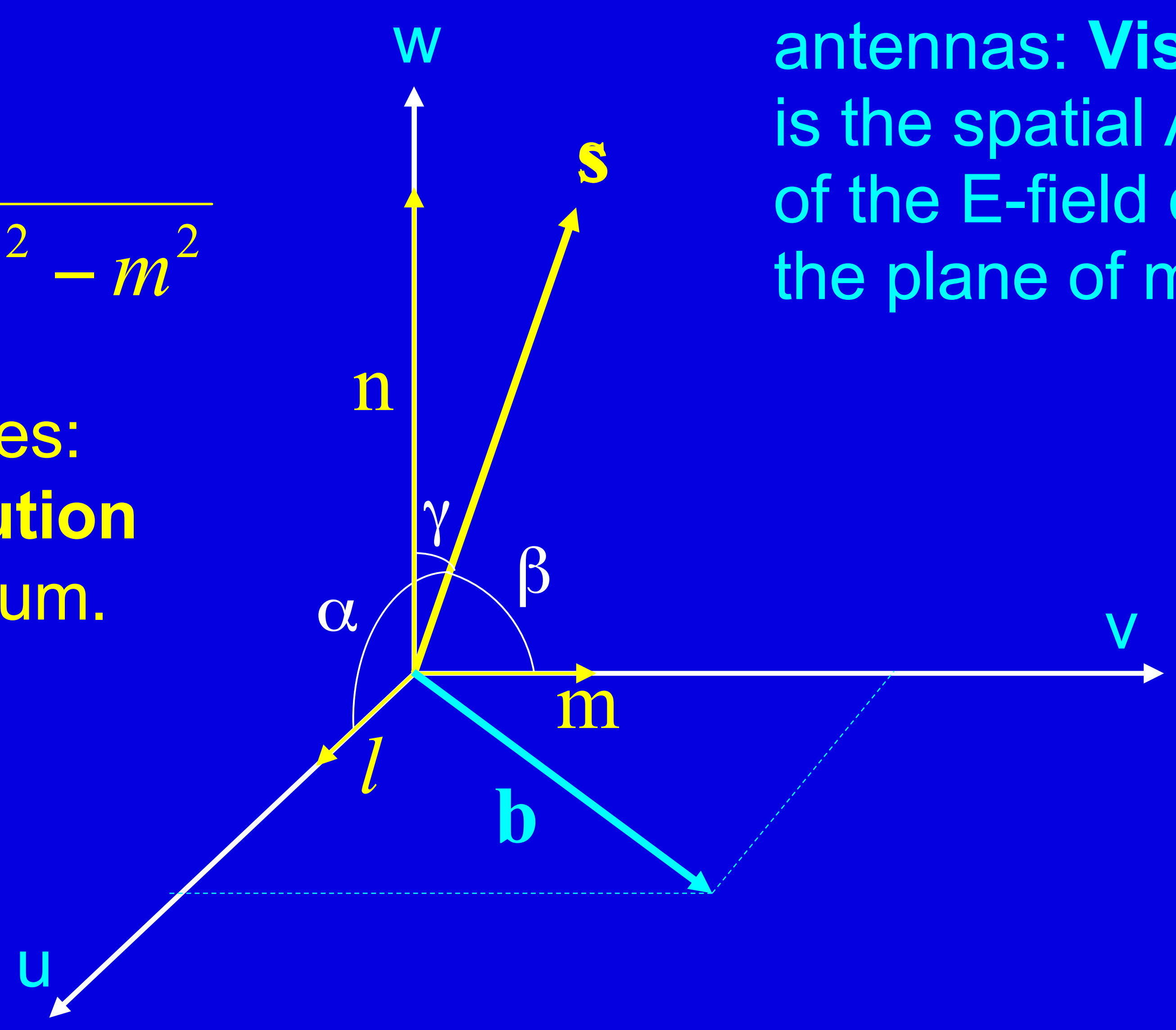

$$\mathbf{B}[\mathbf{s} = (l, m, n)] \xleftrightarrow{\text{Fourier}} \mathbf{V}[\mathbf{b} = (u, v, w)]$$

Aperture Synthesis Imaging Radar ASIR

How it works 2

Aperture Synthesis Imaging Radar ASIR

How it works 2

The Sampling Function $$G(l,m) = \iint S(u,v) e^{2\pi i(ul+vm)} du\, dv$$

Aperture Synthesis Imaging Radar ASIR

How it works 2

The Sampling Function $$G(l,m) = \iint S(u,v) e^{2\pi i(ul+vm)} du\, dv$$

Dirty Brightness $$B_\omega^D(l,m) = \iint V_\omega(u,v) S(u,v) e^{2\pi i(ul+vm)} du\, dv$$

Aperture Synthesis Imaging Radar ASIR

How it works 2

The Sampling Function $$G(l,m) = \iint S(u,v) e^{2\pi i(ul+vm)} du\, dv$$

Dirty Brightness $$B^D_\omega(l,m) = \iint V_\omega(u,v) S(u,v) e^{2\pi i(ul+vm)} du\, dv$$

Deconvolution will be Messy $$B^D_\omega(l,m) = B_\omega \star G$$

Aperture Synthesis Imaging Radar ASIR

How it works 2

The Sampling Function

$$G(l,m) = \iint S(u,v)e^{2\pi i(ul+vm)}du\,dv$$

Dirty Brightness

$$B_\omega^D(l,m) = \iint V_\omega(u,v)S(u,v)e^{2\pi i(ul+vm)}du\,dv$$

Deconvolution will be Messy

$$B_\omega^D(l,m) = B_\omega \star G$$

This is a Singular operation

$$V_\omega(u,v) = \frac{V_\omega^D(u,v)}{S(u,v)}$$

Image inversion/restoration

* Samples of the visibility are uneven, sparse and truncated.
* Inversion is a highly singular problem.
* Needs carefully crafted algorithms to pick out an acceptable solution out of a large space of solutions.
* Then Maximum Entropy Method MEM has been chosen and implemented/tested.

$$\mathcal{H} = -\sum_k B_k \ln \frac{B_k}{eM_k}$$

$$E[f(e_j, \lambda_j, \Lambda, L)] = S + \lambda_j(g_j + e_j - f_i h_{ij}) + \Lambda(e_j^2 \sigma_j^{-2} - \Sigma) + L(I_i f_i - F)$$

Hysell & Chau, Radio Sci. 2006

Five-Baseline Interferometer

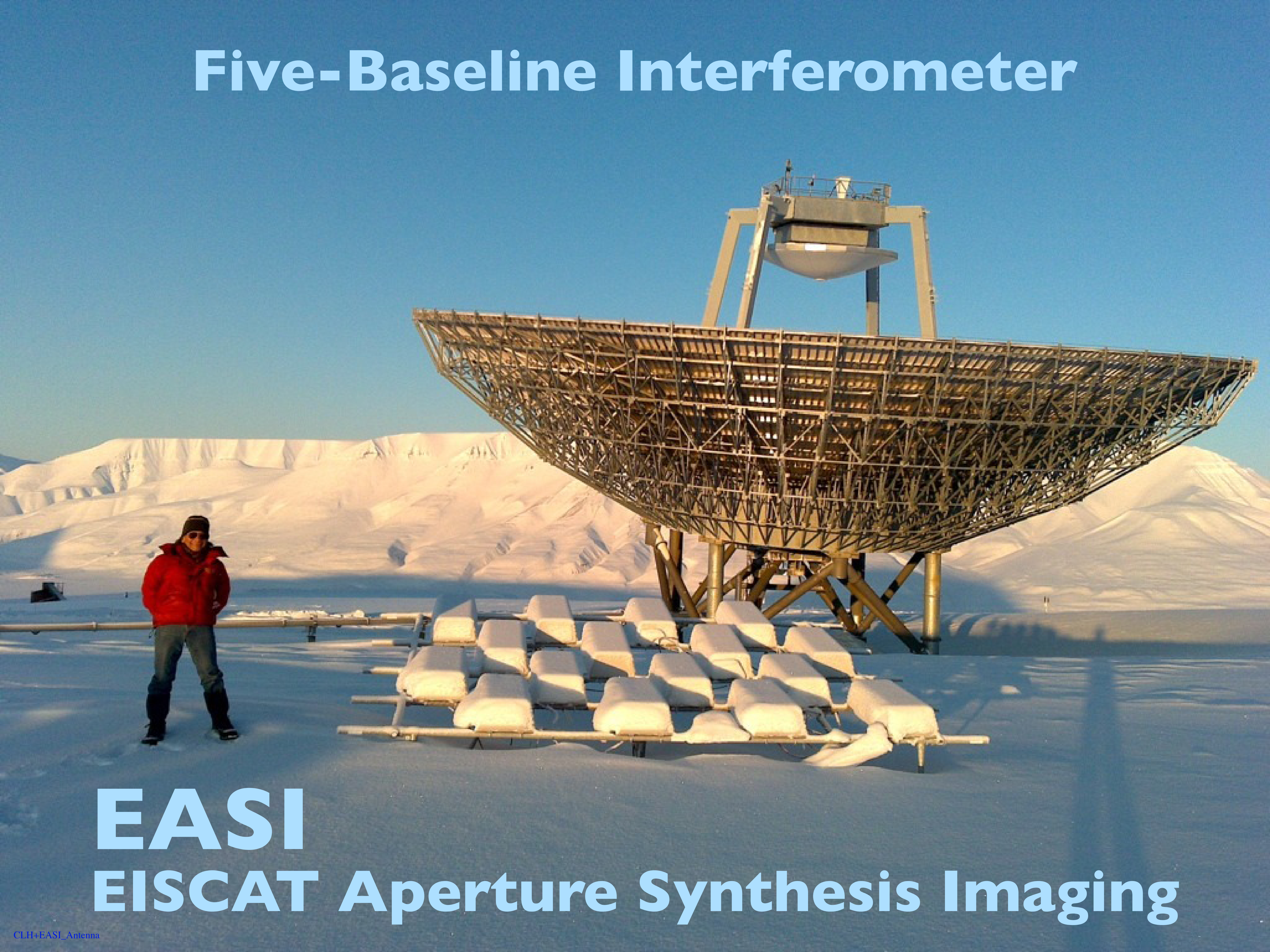

EASI
EISCAT Aperture Synthesis Imaging

CLH+EASI_Antenna

Implementation & validation of MEM inversion

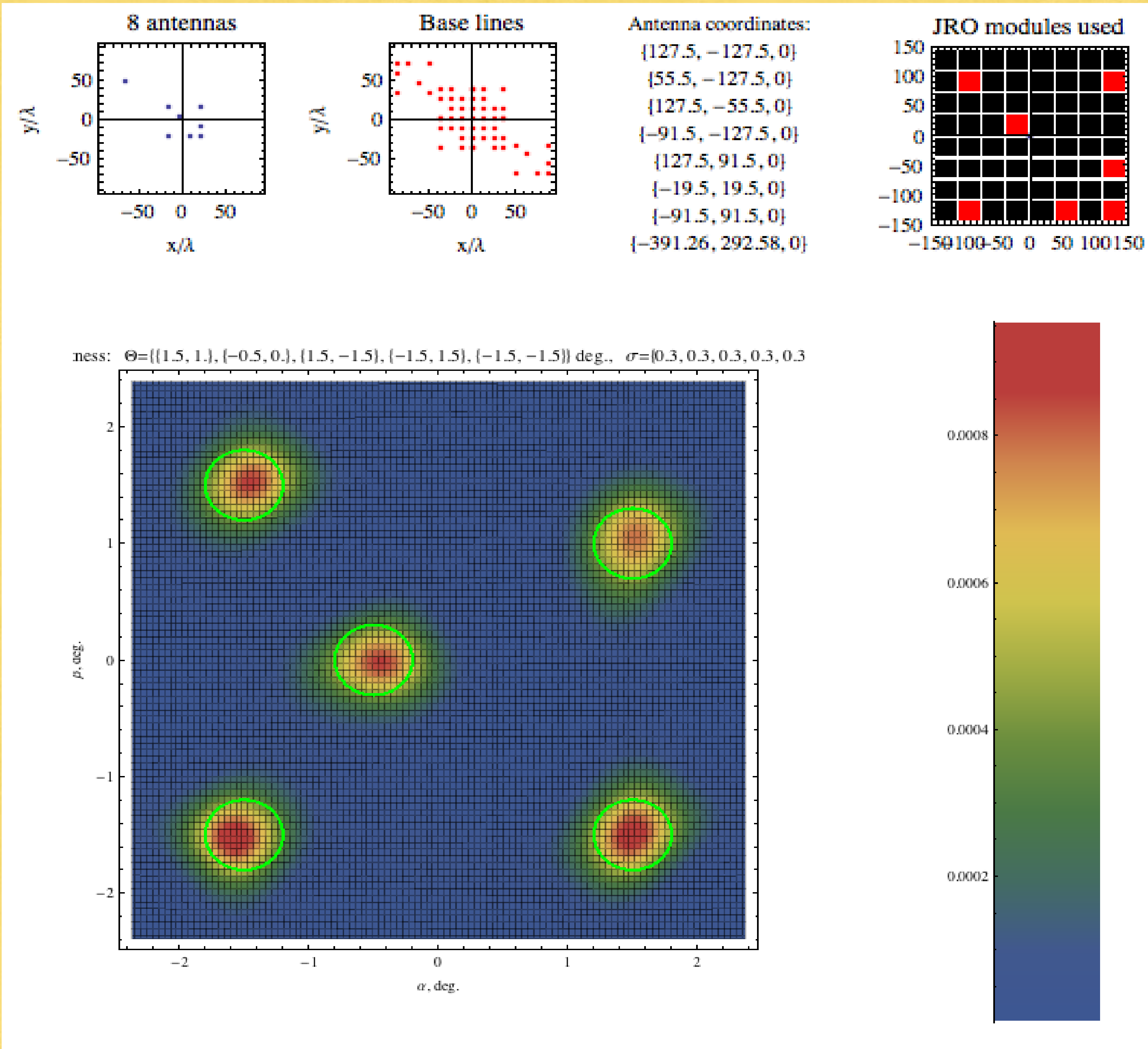

Figure 3. Five-blob image reconstructed from the visibility measured with the 8-antenna configuration with 7 core antennas of the Jicamarca array and 1 outlier shown in the upper left panel. The second upper left panel shows the baselines generated by the configuration. The right most upper panel shows the core antennas used in the configuration in red and their coordinates alongside. It is a remarkably optimum configuration that produces an excellent reconstruction.

Work in progress: Measurements of satellites …

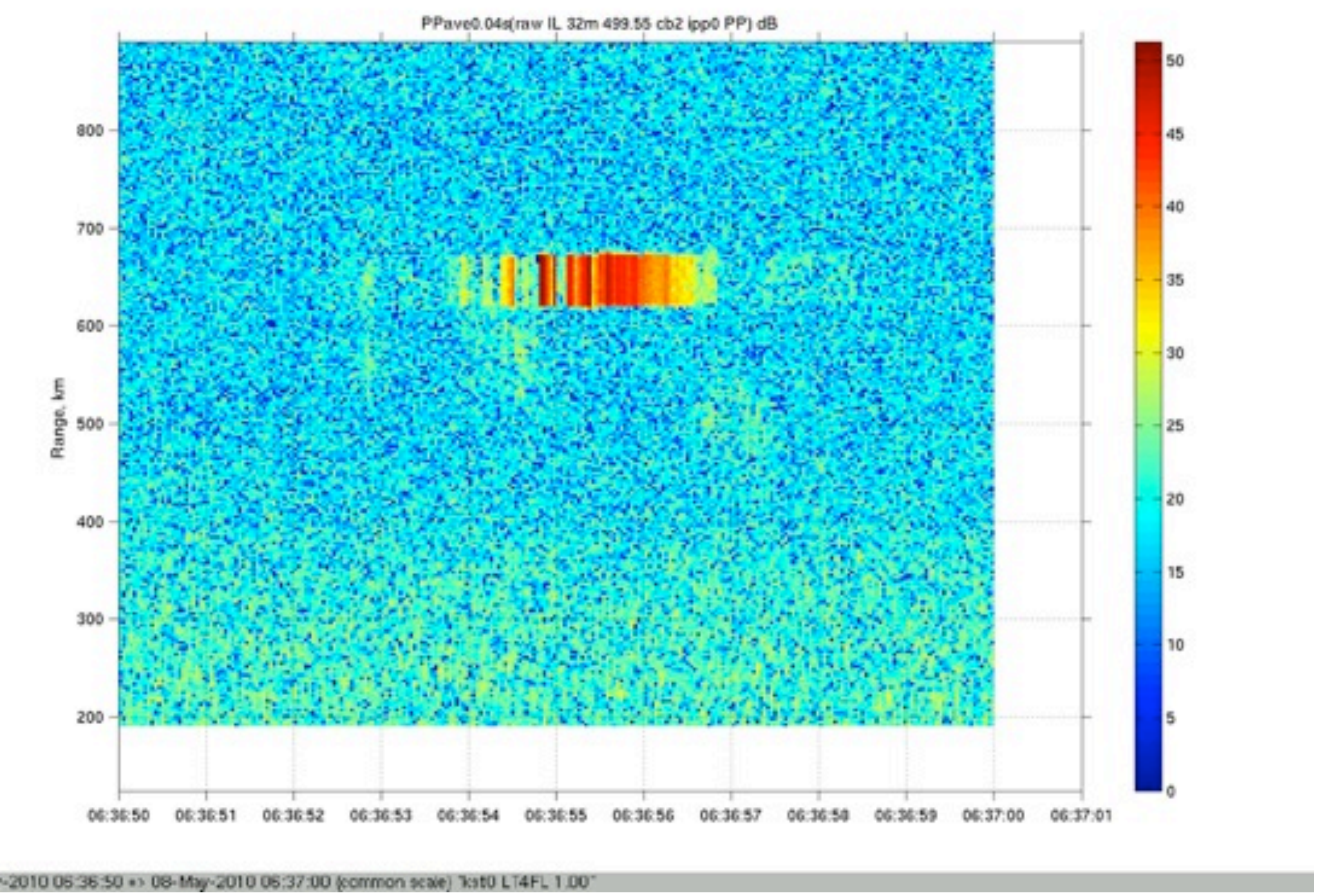

Work in progress: Measurements of satellites …

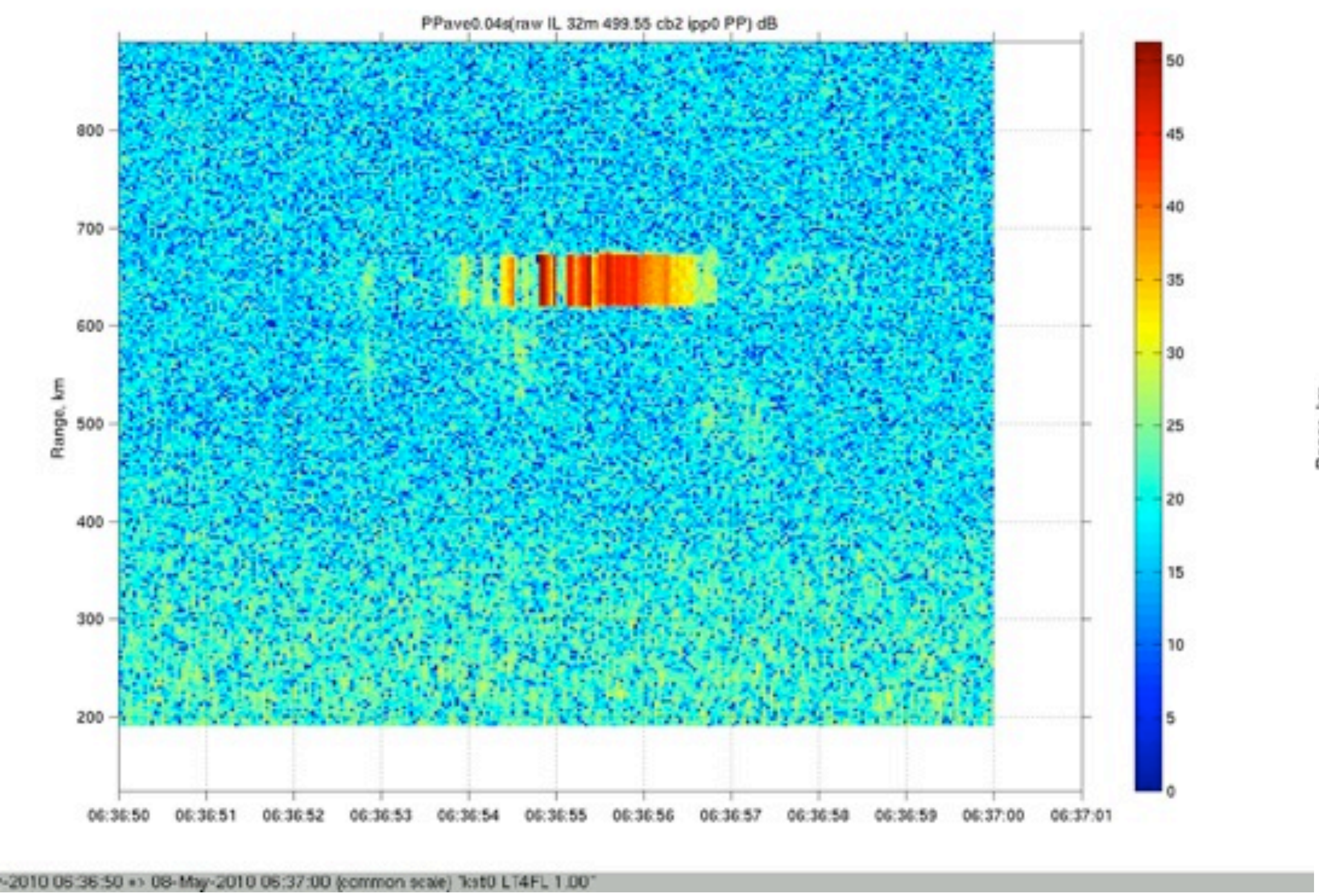

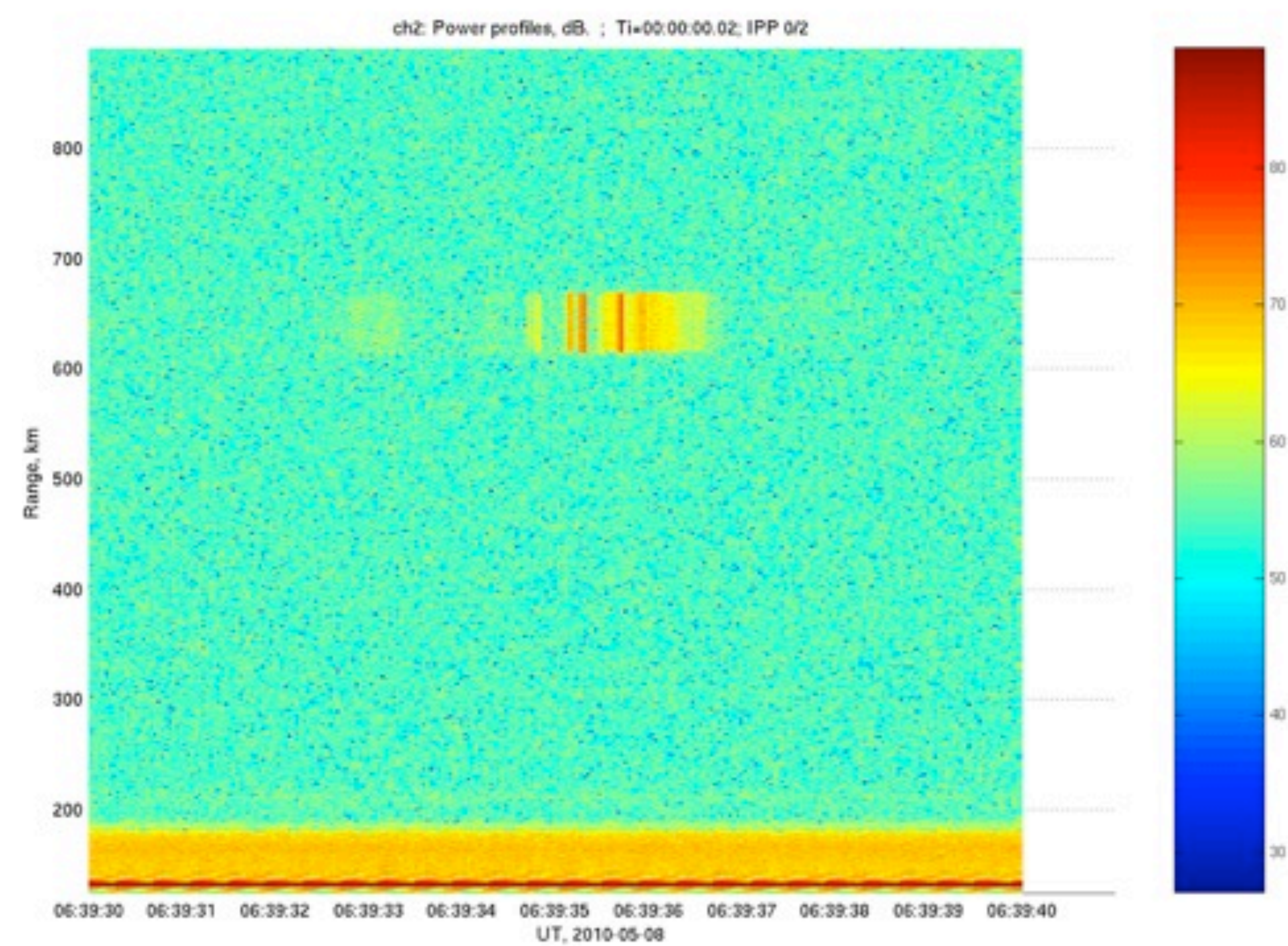

Inversion of a simulated filament

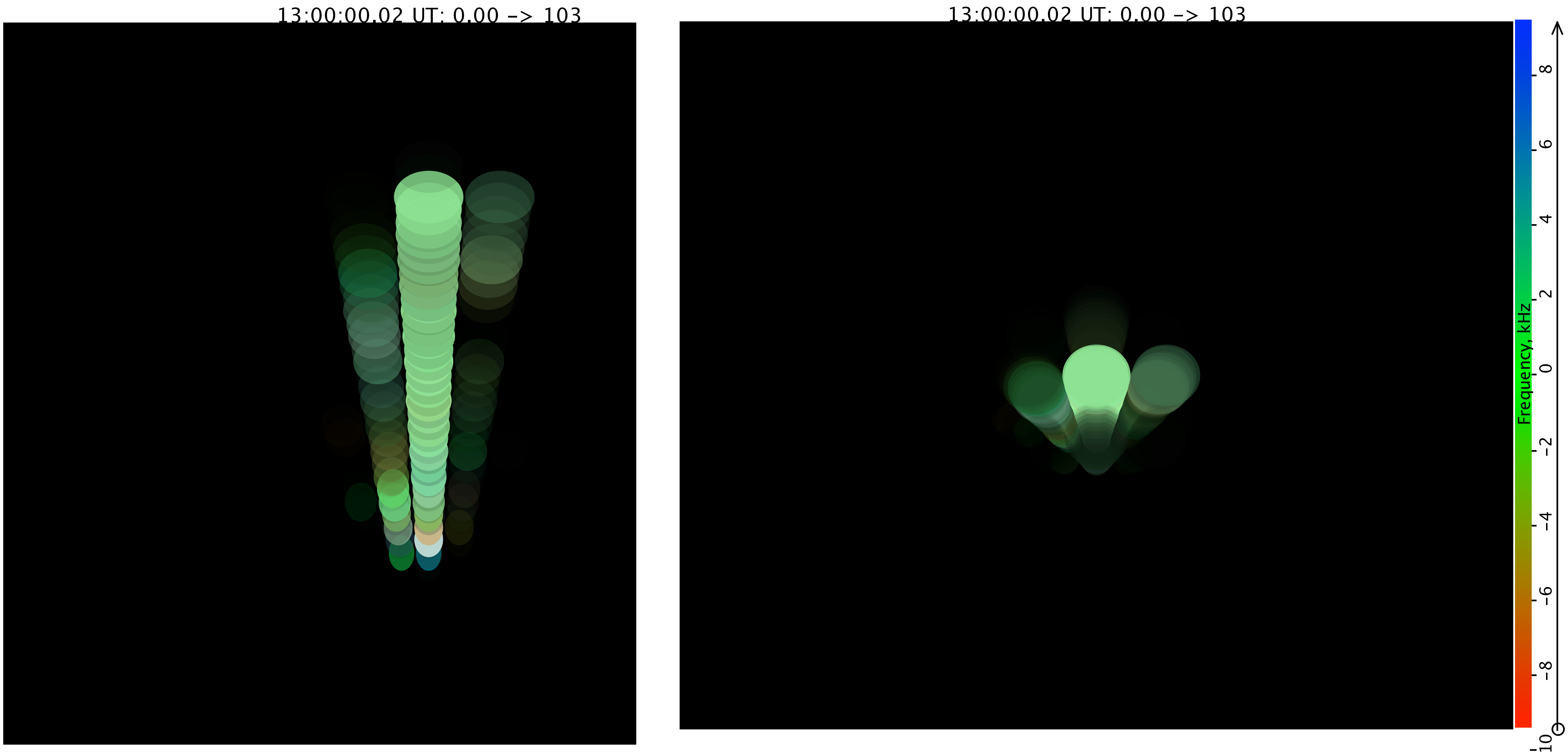

EISCAT_3D
(Vasyl+ Unni+ Asgeir+ Hannah)

EISCAT_3D

EISCAT_3D

European Strategy Forum
on Research Infrastructures

ESFRI

The EUROPEAN Next-Generation Incoherent Scatter Radar

Chosen in 2008 to the ESFRI Roadmap of Large-Scale European Research Infrastructures for the next 20-30 years

EUROPEAN ROADMAP
FOR RESEARCH
INFRASTRUCTURES

Roadmap 2008

European Strategy Forum
on Research Infrastructures

ESFRI

Strategy Report
on Research Infrastructures

Roadmap 2010



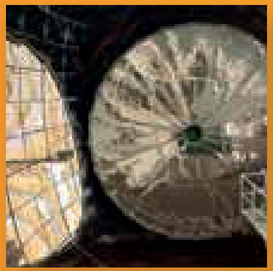
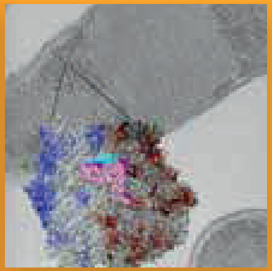

The landscape and its projects

Roadmap 2010

European Strategy Forum on Research Infrastructures

ESFRI

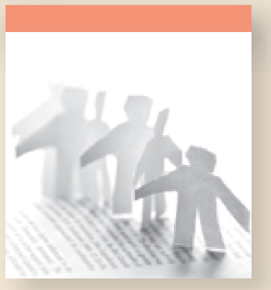

SOCIAL SCIENCES AND HUMANITIES

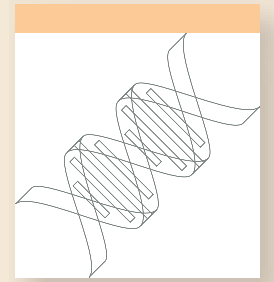

BIOLOGICAL AND MEDICAL SCIENCES

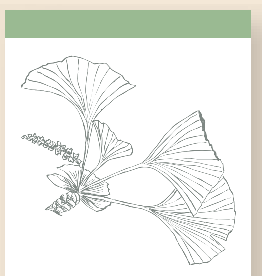

ENVIRONMENTAL SCIENCES

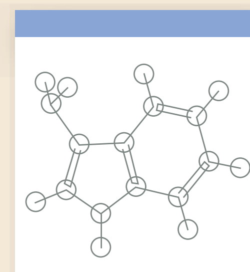

MATERIALS AND ANALYTICAL FACILITIES

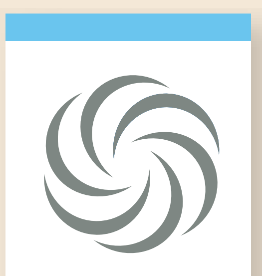

ENERGY

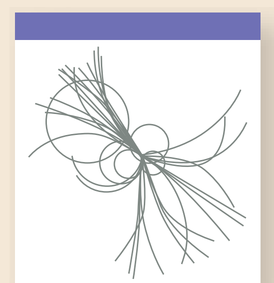

PHYSICAL SCIENCES AND ENGINEERING

The landscape and its projects

Roadmap 2010

European Strategy Forum
on Research Infrastructures

ESFRI

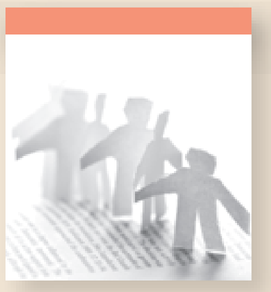

SOCIAL SCIENCES AND HUMANITIES

EISCAT_3D

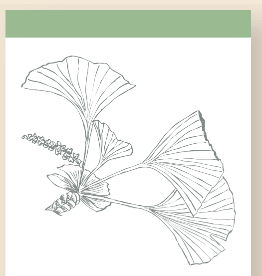

ENVIRONMENTAL SCIENCES

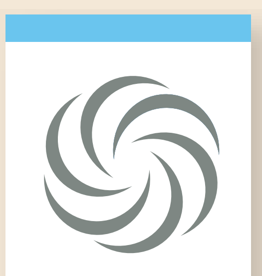

ENERGY

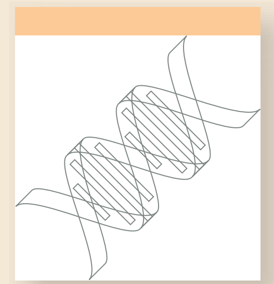

BIOLOGICAL AND MEDICAL SCIENCES

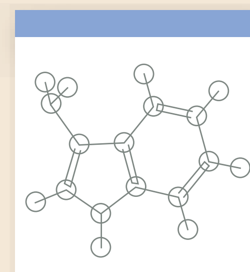

MATERIALS AND ANALYTICAL FACILITIES

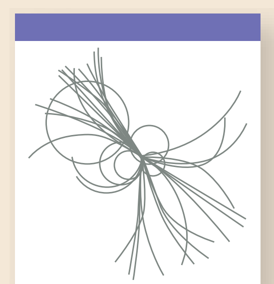

PHYSICAL SCIENCES AND ENGINEERING

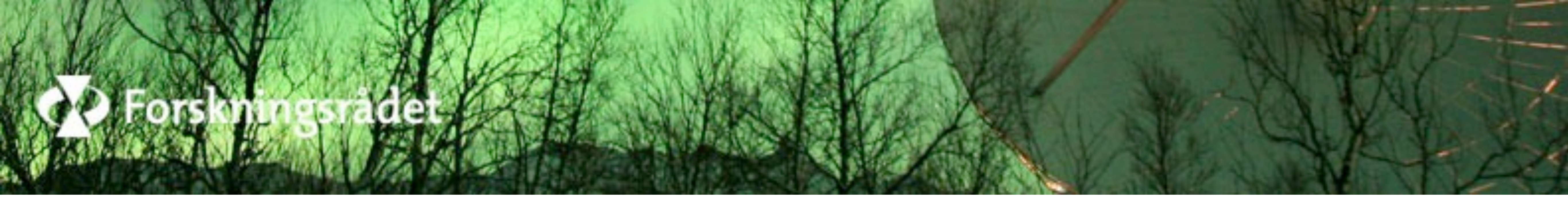

UTLYSNING

300 millioner kroner til forskningsinfrastruktur

Midler til forskningsinfrastruktur (INFRASTRUKTUR) er nå utlyst. Utlysningen blir aktiv seks uker før søknadsfrist 17. oktober.

Midlene skal gå til forskningsinfrastruktur av nasjonal karakter, inkludert norsk deltakelse i fremtidig internasjonal infrastruktur (som ESFRI). Utlysningen er åpen, men med en begrenset økonomisk ramme vil fire forskningspolitiske prioriteringer vektlegges ved utvelgelsen av prosjekter.

Klikk her for full utlysningstekst

EISCAT_3D-NORGE
søknad sendt
17 October 2012

Skrevet av: Richard Trondstad Susegg

Publisert: 18.06.2012
Sist oppdatert: 18.06.2012

A proposal to the Research Council of Norway

- University of Tromsø (UiT)
- University of Bergen (UiB)
- University of Oslo (UiO)
- The University Centre at Svalbard (UNIS)
- Norwegian University of Science & Technology (NTNU)
- Andøya Rocket Range (ARR)
- Norwegian Space Centre (NSC)

Summary

This proposal is asking for Norwegian funding towards construction of EISCAT_3D (E3D), which is an international project on The European Strategy Forum on Research Infrastructures (ESFRI) roadmap. E3D is a world-class radar facility for investigations of the geospace environment. It will replace the ageing EISCAT facilities in northern Norway, Sweden and Finland. E3D will use the incoherent scattering (IS) technique to make 3-dimensional vector measurements across a wide field of view of key parameters in the auroral atmosphere by taking advantage of technological advances in radio, radar, computing, and signal analysis. E3D will have 20 times better sensitivity and one order of magnitude better resolution than all other radar facilities in the world. E3D will allow us to understand the flows, sources, sinks, and interactions of energy, momentum and mass in the auroral atmosphere. E3D will provide synergies towards relevant areas of increasing socioeconomic importance; including atmospheric precursors of climate change and vulnerability of modern technological infrastructures due to space weather and space debris. E3D can study auroral particle precipitation that depletes ozone in the stratosphere, and atmospheric tides and sudden stratospheric warming events that bring disturbances to the ionosphere from below. Real-time measurements from E3D will be provided to monitoring services dealing with space weather and space debris, a key focus of ESA's Space Situational Awareness (SSA) programme. E3D will also contribute to science and engineering education at all levels. The project will create opportunities to national industry and services in communications hardware and software and information technologies. This E3D project is backed by all major universities in Norway (Tromsø, Bergen, Oslo, UNIS and NTNU), Andøya Rocket Range, and the Norwegian Space Centre.

1. Relevance to the Call for Proposals

Norway has been a leading member of the EISCAT Scientific Association for over 30 years being home to its most substantial facilities. Three generations of Norwegian scientists have obtained their education using EISCAT and some have made their career in the EISCAT organisation. This is no coincidence, since Northern Norway lies right under the oval where the Northern Lights have mesmerised and puzzled mankind for centuries. The human urge to understand its surroundings is illustrated by Kristian Birkeland's (1867-1917) astonishing curiosity-driven creativity to unravel nature's riddles presented before his eyes (see picture). Although many of the processes in the Aurora Borealis are well known, there is still debate regarding important details. Auroral forecasts are still primarily empirical, mostly qualitative and unreliable. We have just begun to realise how violent auroral storms may threaten our modern technology. Climate researchers also provide growing evidence that the entire Arctic region is in rapid transition, which will also affect layers in the atmosphere.

EISCAT_3D (E3D) is in The European Strategy Forum on Research Infrastructures (ESFRI) roadmap. It will be a world-class radar facility for studies of high-latitude geospace[1] science and space plasma physics. The ultimate raison d'être of E3D is motivated by Kristian Birkeland's urging. Technological advances in radio, radar, computing, and signal analysis open new opportunities. With twenty times better sensitivity and one order of magnitude better resolution in time and space, E3D will replace the ageing EISCAT facilities in northern Norway, Sweden and Finland. E3D will restore Europe's technological and scientific lead in ground-based investigation of geospace.

2. Vision and Scientific Goals

- Our vision is to understand the geospace environment at auroral latitudes in 3-Dimensions for the benefit of modern society.

- E3D is the research infrastructure to achieve our vision, allowing us to understand the flows, sources, sinks, and interactions of energy, momentum and mass in the auroral atmosphere.

- Our vision unfolds into several non-exhaustive key challenges that we will endeavour to respond to using E3D:

EISCAT_3D Norway Science Questions

Q1 How to proceed beyond the present simplistic, static, stationary and homogeneous analysis of upper atmospheric and ionospheric processes?

Q2 How does space weather affect ionospheric processes and how to support modelling and space weather services?

Q3 How to advance fundamental plasma physics by employing the ionosphere as a natural plasma physics laboratory?

Q4 How does the influx of extraterrestrial material interact with the upper atmosphere and where does the material originate from?

Q5 How does solar activity couple from geospace into the lower atmosphere and climate system, and does this energy change the wave forcing of geospace from below?

Answer: EISCAT_3D

The Instrument

Table 1 **EISCAT_3D Specifications**

	Transmitter		
1	Type	Pulsed	-
2	Duty Cycle	25	%
3	Max Pulse Length	10	ms
4	Shortest Pulse Length	0.5 (75)	μs (m)
5	Peak Power	10	MW
6	Centre frequency	233	MHz
7	3 dB Bandwidth	$\pm$2.5	MHz
8	Modulation	Phase/Amp	-
9	Polarization	Arbitrary	-
	Antennas		
10	Type	Phased Array	-
11	Antennas per site	$\sim$10,000	-
12	3 dB Bandwidth	$\pm$15	MHz
13	Gain	$\sim$50	dBi
14	beam pointing resolution	0.625°	
15	Transverse resolution at 100 km better than	50	m
16	Grating-lobe free radiation pattern: zenith all azimuths	40°	
17	Power-aperture product	>100	GWm^2

	Features	
1	3-dimensional vector and scalar imaging	*
2	Phase/Amp transmitter modulation	*
3	Arbitrary Tx/Rx polarisation	
4	One Core Active site	
5	4 Remote Passive sites	
6	Remote active site with power $\sim$1 MW	
7	Electronic scanning and beam-forming	
8	5 phased steered array antennas	
9	6-10 outlying antenna arrays at active site	
10	Aperture synthesis imaging	
11	High duty cycle	
12	Better sensitivity by a factor > 20×	**
13	Unmanned operation	
14	Remote operation via internet	
15	Robust reliability in arctic environment	
16	Uninterrupted continuous operations	
17	Common Programs at low duty cycle	
18	Special Programs to respond to pre-defined/unusual geophysical events	
19	Validated archival database	
20	Restricted real-time data	

* Unique Technological Innovation

** Major Improvement

Essential Features to attain the Scientific Goals

The Hardware

E3D Cost Breakdown						
Unit	Units	Unit Cost	Total	Unit Cost	Total	
		T/R Array		R Array		
		€	M€	€	M€	
Antennas Tx	10000	390	3.9			
Transmitters Tx	20000	1600	32.0			
Antennas Rx	10000	300	3.0	300	3.0	
Receivers Rx	20000	340	6.8	340	6.8	
Comps/Comms	1		3.5		3.5	
Infrastructure	1		2.0		1.5	
Site/Work	1		3.5		2.2	Total M€
Cost/Array			54.7		17.0	122.7

Investment Profile

E3D Funding & Investment Profile								
Preparation			Construction			Commision		
2014	2015	2016	2017	2018	2019	2019	2019	
Investment Profile M€								Total M€
4	32	35	33	16	4	4	4	132
Operations Costs M€								
3.4	6.0	7.0	7.2	8.3	8.7	9.2	9.3	
Investment from this proposal M€								Total M€
3	8	10	6	2				29

Norway

NFR Søknad

MNOK 213.7

EISCAT_3D: Candidate Sites

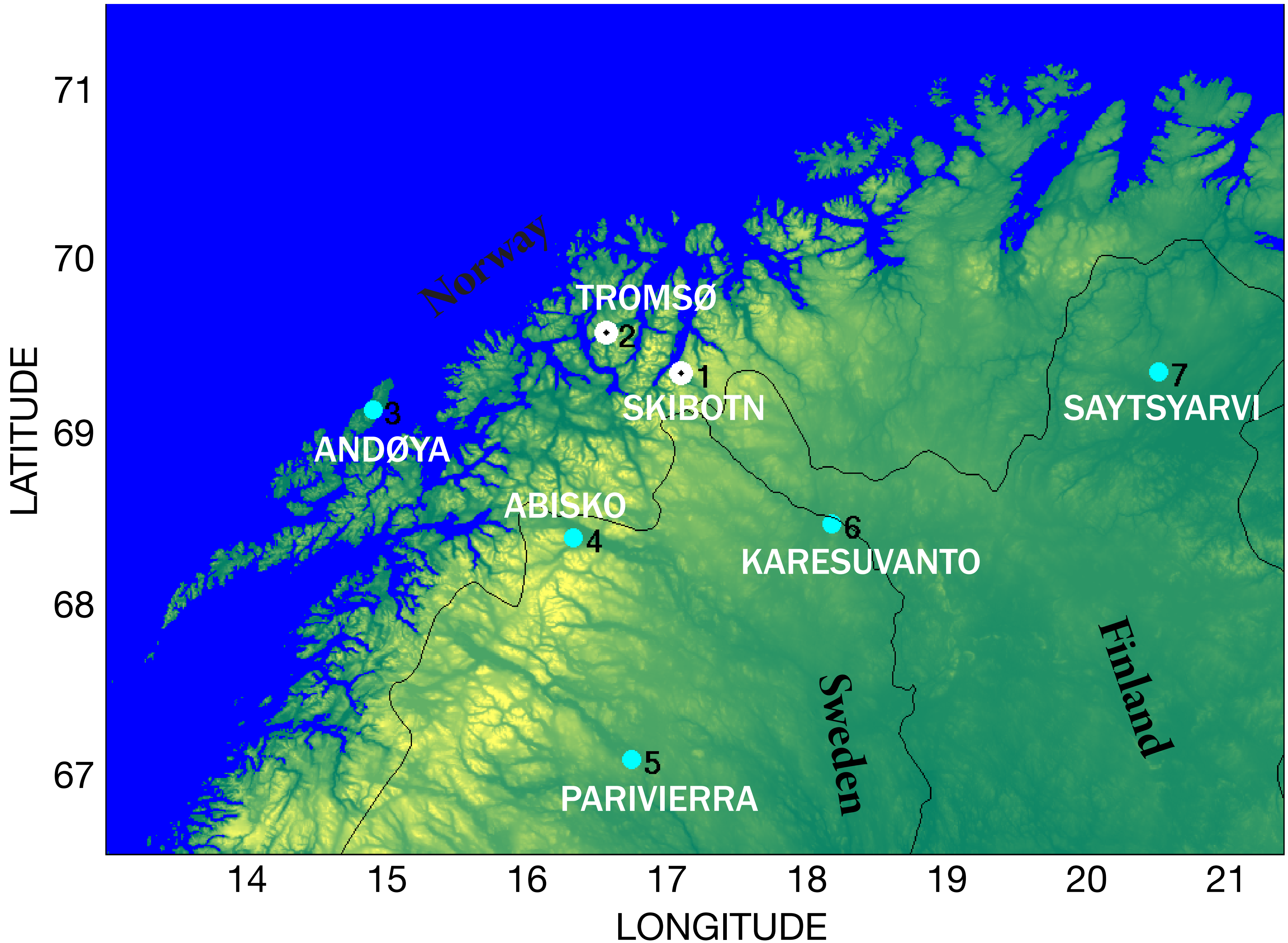

Transmit/Receive ● Receive only ●

EISCAT_3D Norway: Letters of Support

University of Tromsø

1

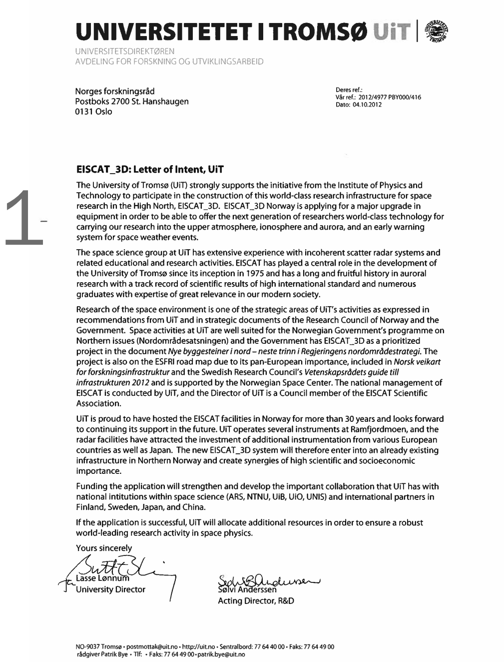

EISCAT

2

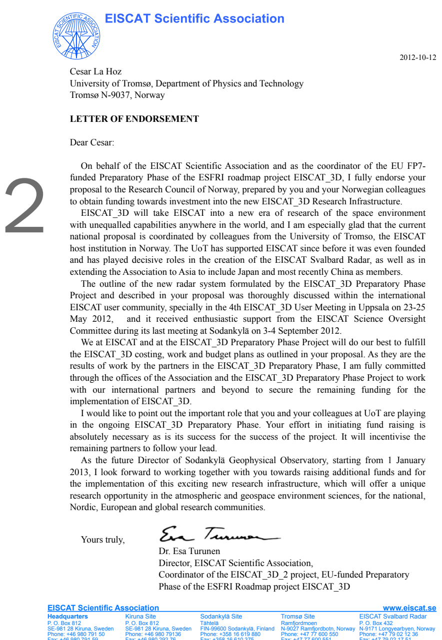

University of Bergen

3

University of Oslo

4

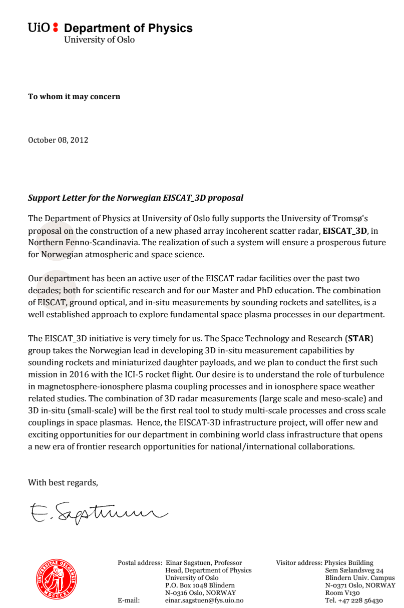

UNIS

5

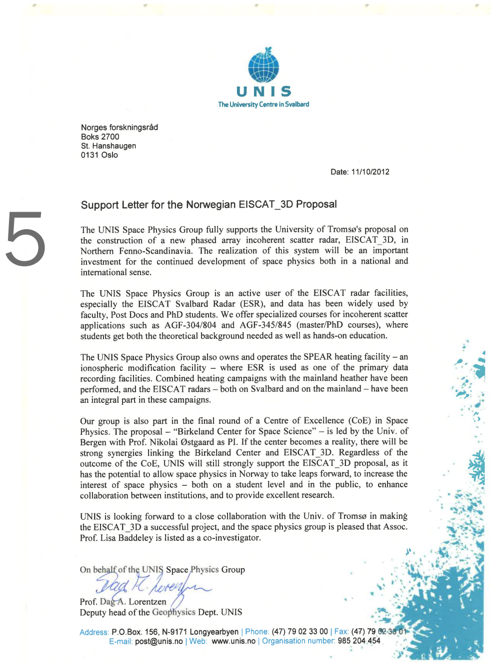

NTNU

6

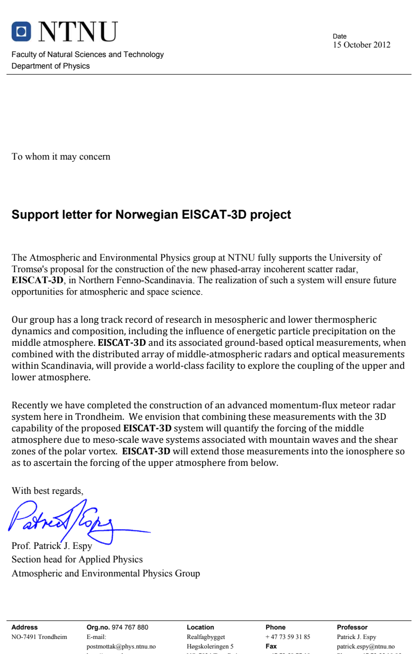

Norwegian Space Centre

7

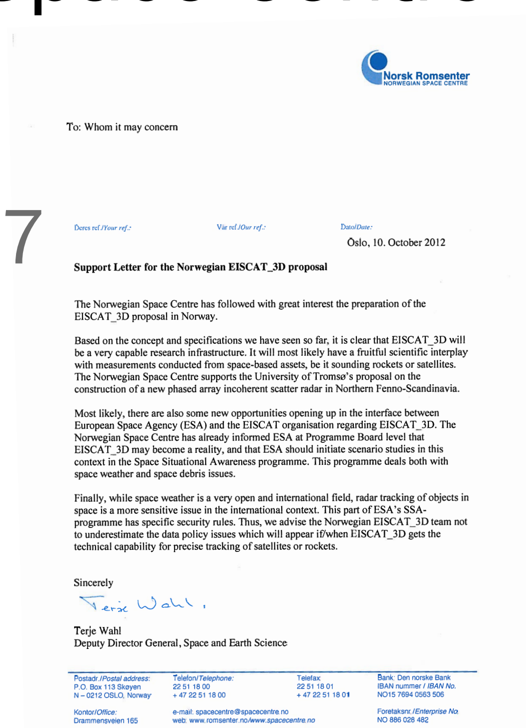

EISCAT Council Chairman

8

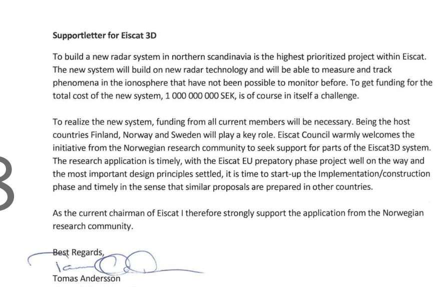

SuperDarn

9

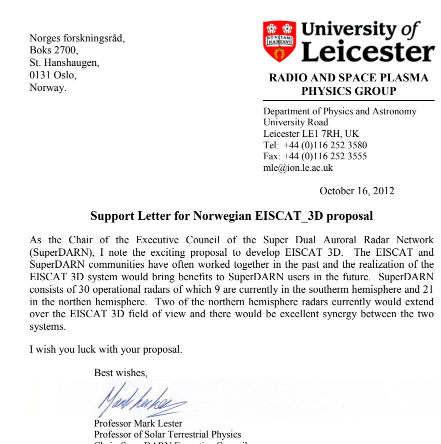

EISCAT_3D Norway: Consortium Building

•Trondheim:	29 Feb – 1 Mar	24
•Bergen:	28 - 29 June	18
•Geilo:	11 - 12 September	12
•Sommarøya	30 Sept. – 2 Oct.	10
•Tromsø	8 - 9 October	4
•Submitted	17 October	

E3DN Consortium

Everyone

EISCAT
EISCAT_3D

- EISCAT started in 1976-1981: more than 30 years
- Norway (UiT) founder from the beginning
- 3rd Generation most advanced IS radar: Tristatic
- 3 generations of Norwegians educated/worked in EISCAT (>62)
- Is in the elite of the world IS radar facilities
- International prestige to UiT, Tromsø, Norway, Europe
- World class science production in geospace research
- Norway has paid one, got two-four in return
- The largest international research infrastructure in Norway
- UiT, UiO, UiB, UNIS, ARS, future NTNU users of EISCAT

WE HAVE A RESPONSIBILITY TO PRESERVE EISCAT

EISCAT_3D Norway (E3DN) Project

Three Generations of EISCAT in Norway

October 2012

1	Olav Holt	UiT	32	Hilde Nesse Tyssøy	UiB
2	Tor Hagfors	NTH	33	Morten Blixt	UiT
3	Asgeir Brekke	UiT	34	Anja Strømme	UiT
4	Egil Leer	UiT	35	Bjørn Gustavsson	UiT
5	Kristen Folkestad	FFI	36	Vasyl Belyey	UiT
6	Per Simon Kildal	NTH	37	Eirik Malnes	UiT
7	Jan Trulsen	UiT	38	Frank Melandsø	UiT
8	Kristian Dysthe	UiT	39	Alvin Brattli	UiT
9	Noralv Bjørnå	UiT	40	Øyvind Pettersen	UiT
10	Ove Havnes	UiT	41	Torsten Aslaksen	UiT
11	Einar Mjølhus	UiT	42	Lars Næsheim	UiT
12	Kristoffer Rypdal	UiT	43	Kjellmar Oksavik	UiB
13	Truls Hansen	UiT	44	Dag Lorentzen	UNIS
14	Johan Stadsnes	UiB	45	Lisa Baddeley	UNIS
15	Finn Søraas	UiB	46	June Lunde	UiT
16	Cesar La Hoz	UiT	47	Magnar Gullestad Johnsen	UiT
17	Kjartan Olafsson	UiB	48	Baily	UiT
18	Trygve Sparr	UiT	49	Essayas	UiT
19	Chris Hall	UiT	50	Endawoke Yizengaw	UiT
20	Tor Flå	UiT	51	Yvonne Rinne	UiO
21	Unni Pia Løvhaug	UiT	52	Solomon Kebede	UiT
22	Åshild Fredriksen	UiT	53	Hannah Vickers	UiT
23	Jøran Moen	UiT	54	Henry Pinedo	UiT
24	Alfred Hanssen	UiT	55	Vigdis Lonar Barth	UiO/UNIS
25	Patrick Guio	UiT	56	Karina E. B. Ibanez	UiO/UNIS
26	Nikolai Østgaard	UiB	57	Åsmund Skjæveland	UiO/UNIS
27	Arve Aksnes	UiB	58	Christer Van Der Meeren	UiB
28	Tom Grydeland	UiT	59	Christoffer Stausland	UiO
29	Gard Skauge	UiB	60	Meseret Kassa	UiT
30	Trond Trondsen	UiT	61	Alexander Bibriecher	UiT
31	Ruth Esser	UiT	62	Lindis Bjoland	UiB